The beta 2 adrenergic receptor cross-linked interactome identifies 14-3-3 proteins as regulating the availability of signaling-competent receptors

Ian B. Chronis, Rachel Vistein, Avanti Gokhale, Victor Faundez, Manojkumar A. Puthenveedu

IBC, MAP: Department of Pharmacology, University of Michigan Medical School, Ann Arbor, Michigan.

RV: Department of Molecular and Comparative Pathobiology, Johns Hopkins School of Medicine, Baltimore, Maryland.

AG, VF: Department of Cell Biology, Emory University School of Medicine, Atlanta, Georgia.

14-3-3 proteins regulate adrenergic receptor reserve

Corresponding author: Manojkumar Puthenveedu

Address

Medical Science 1 3422D

1301 Catherine Street

Ann Arbor, MI

48109

Phone number: 734-936-6640

Email address: puthenve@umich.edu

Number of text pages: 32

Number of tables: 0

Number of figures: 8

Number of references: 97

Number of words

Abstract: 217

Introduction: 598

Discussion: 1500

List of non-standard abbreviations

ANOVA	analysis of variance
APEX	engineered ascorbate peroxidase
AUC	area under the curve
B2AR	beta 2 adrenergic receptor
CCC	COMMD/CCDC22/CCDC93
CORVET	class C core endosomal vacuole tethering
DSP	dithiobis(succinimidyl proprionate)
ERK	extracellular signal-regulated kinase
GO	gene ontology

2

GPCR	G protein-coupled receptor
HA	hemagglutinin
HEK293	human embryonic kidney 293
ICL	intracellular loop
PDE	phosphodiesterase
PKA	protein kinase A
pLDDT	predicted local distance difference threshold
SILAC	stable isotope labeling by amino acids in cell culture
SPH	supercleptic pHluorin
YFP	yellow fluorescent protein

Abstract

The emerging picture of G protein-coupled receptor function suggests that the global signaling response is an integrated sum of a multitude of individual receptor responses, each regulated by their local protein environment. The beta 2 adrenergic receptor (B2AR) has long served as an example receptor in the development of this model. But the mechanism and the identity of the protein-protein interactions that govern the availability of receptors competent for signaling remains incompletely characterized. To address this question, we characterized the interactome of agonist-stimulated B2AR in HEK293 cells using FLAG co-immunoprecipitation coupled to SILAC labeling and mass spectrometry. Our B2AR cross-linked interactome identified 190 high-confidence proteins, including almost all known interacting proteins and six out of seven isoforms of the 14-3-3 family of scaffolding proteins. Inhibiting 14-3-3 proteins with the peptide difopein enhanced isoproterenol-stimulated adrenergic signaling via cAMP approximately three-fold, and increased both miniGs and arrestin recruitment to B2AR more than two fold each, without noticeably changing EC50 with respect to cAMP signaling or effector recruitment upon stimulation. Our results show that 14-3-3 proteins negatively regulate downstream signaling by inhibiting access of B2AR to effector proteins. We propose that 14-3-3 proteins maintain a dynamic pool of B2AR that has reduced signaling efficacy in response to acute agonist stimulation, limiting the amount of signaling-competent receptors at the plasma membrane.

Significance Statement

This study presents a new interactome of the agonist-stimulated beta 2 adrenergic receptor (B2AR), a paradigmatic GPCR that is both a model system for members of this class and an important signaling protein in respiratory, cardiovascular, and metabolic regulation. We identify 14-3-3 proteins as responsible for restricting B2AR access to signaling effectors and maintaining a receptor population that is insensitive to acute stimulation by agonists.

Introduction

The beta 2 adrenergic receptor (B2AR)–a prototypical member of the G protein-coupled receptor (GPCR) family–has long been a physiologically relevant in our understanding of GPCR function. GPCRs recognize and respond to a variety of extracellular signals, and initiate multiple intracellular signaling pathways that integrate to generate a physiological response (Pierce *et al.*, 2002). Because of the variety and specificity of GPCRs they have been historically used as a major target for drug development, and a large percentage of available drugs target aspects of their signaling (Sriram and Insel, 2018). B2AR was among the first GPCRs identified and has long been used as a canonical example (Bylund, 2006; Lefkowitz, 2007).

Our understanding of how B2AR agonists generate a complex downstream cellular response is still evolving. The primary pathway initiated by B2AR activation increases the second messenger cAMP via activation of adenylyl cyclase by Gαs protein (Johnson, 1998). B2AR can also activate several other pathways, such as the MAP Kinase pathway, presumably by multiple mechanisms independent of cAMP (Shenoy *et al.*, 2006; O'Hayre *et al.*, 2017; Kwon *et al.*, 2022). Emerging evidence reveals that the global cellular response to B2AR activation is the summation of a large number of tightly controlled responses from individual receptors, each of which could be different in efficacy, specificity, and timing, depending on the immediate environment of the receptor (Anton *et al.*, 2022).

One interesting aspect of B2AR activation is that agonists can generate maximal activation of second messengers, as measured by traditional assays, despite activating only a subset of available receptors (Terasaki *et al.*, 1979; Venter, 1979; Drury *et al.*, 1998; Giembycz, 2009). This saturation could be caused by fundamental properties of the receptor signaling cascade at multiple levels. It is well established that signal amplification, in a system where downstream

6

components are limiting, could generate maximal cellular or tissue-level effects even if only a fraction of receptors are activated (Buchwald, 2019). In addition, variations in the intrinsic efficacy of individual drug-receptor complexes could also contribute to saturation, if a portion of receptors are held in a state that is not capable of initiating signaling cascades. However, whether and how B2AR can be sequestered into signaling-incompetent pools at the plasma membrane is not fully understood.

The most likely possibility is that variations in signaling efficacy and outputs of individual receptors are determined by different arrays of effector and regulatory proteins that are present in the immediate environment of individual receptors. Subsets of B2AR could therefore interact with different proteins, with their particular protein interactions regulating the ability of the receptor to respond to stimuli, as well as the particular signaling pathways through which they do so. To better understand the mechanisms of B2AR activation and regulation, and to determine the downstream effectors of B2AR-mediated signaling pathways, it is important to identify the receptor interactome and how the interactome determines signaling outputs by B2AR.

Here we focused on the interactome of B2AR by taking an unbiased, exploratory approach. We used stable isotope labeling by amino acids in cell culture (SILAC) coupled to cross-linked co-immunoprecipitation and quantitative mass spectrometry to identify proteins associated with activated B2AR. This approach was validated by identification of previously-characterized B2AR interactors, as well as a substantial number of novel interactions with known functions in the endosomal system and receptor trafficking. We identified 14-3-3 proteins as agonist-regulated B2AR interacting proteins that negatively regulate the amplitude of B2AR-initiated cAMP production and association with arrestin, without affecting ERK signaling. Our results provide a rich dataset of B2AR interacting proteins, and suggest a model where 14-3-3 could regulate the

7

availability   of   signaling-competent   B2AR.

Materials and Methods

Plasmids

SSF-B2AR is human B2AR preceded by a signal sequence and FLAG epitope, as has been described previously (Lauffer *et al.*, 2010). SSF-B2AR-APEX and SSF-B2AR-LgBit were created by restriction enzyme cloning using EcoR1 and Not1 sites to insert APEX2 or LgBit into the B2AR C-terminus after P385, flanked by GSGG linkers. SpH-B2AR is B2AR preceded by the pH-sensitive GFP superecliptic pHluorin (SpH), as has been described previously (Yudowski *et al.*, 2006). HA-14-3-3ε (Addgene,116886) was a gift from Drs. Feng-Qian Li and Ken-Ichi Takemaru (Li *et al.*, 2008). SmBit-miniGs was produced from mVenus-miniGs by replacing mVenus with SmBit using site-directed insertion mutagenesis with Q5 polymerase (NEB), according to the manufacturer's instructions. β-arrestin-SmBit was produced from β-arrestin-GFP by replacing GFP with SmBit using site-directed insertion mutagenesis with Q5 polymerase. YFP-R18 K-mutant and YFP-Difopein have been previously described under the names pSCM138 and pSCM174, respectively (Masters and Fu, 2001). These plasmids were generously provided by Drs. Haian Fu and Qiankun Niu (Emory University School of Medicine). The YFP tag was replaced with mCherry using Gibson assembly cloning to create mCherry-R18 K-mutant and mCherry-Difopein for experiments with SpH, to avoid spectral overlap, and NanoBit experiments where NanoBit bioluminescence could result in resonant energy transfer to YFP.

Cell maintenance and reagents

HEK293 cells were purchased from American Type Culture Collection and maintained in Dulbecco's Modified Eagles Medium, High Glucose (Hyclone, SH3024301) supplemented with 10% fetal bovine serum (Gibco, 26140079) in a 37˚C incubator at 5% carbon dioxide. HEK293 cells stably expressing FLAG-B2AR and SpH-B2AR have been described previously (Yudowski

9

et al., 2006; Lauffer *et al.*, 2010). All transfections were conducted using Effectene (Qiagen, 301425) as recommended by the manufacturer and with a plasmid DNA (ng):enhancer (µL):effectene (µL) ratio of 1:8:25. A clonal cell line stably-expressing SSF-B2AR-APEX was produced by transfecting HEK293 cells in a 12-well dish with 750 ng of the SSF-B2AR-APEX plasmid, then passing cells to 15 cm dishes such that individual cells were sparsely distributed. Cells were treated with 400 µg/mL Zeocin (Invitrogen, R25001) for approximately 14 days, with selection media changed every three days. Once colonies were visible by eye, individual colonies were isolated with plastic cloning rings, cultured, and assayed for construct expression using confocal microscopy.

Isoproterenol hydrochloride (Sigma Aldrich, I5627) was prepared fresh as a 100 mM stock in water and diluted to 100x final concentration in water prior to treatment. For concentration-response curves in cAMP GloSensor and NanoBit assays, isoproterenol treatment was prepared by 10x serial dilution in the relevant assay medium. Forskolin (Sigma Aldrich, F3917) was prepared as a 10 mM stock solution in DMSO before being aliquoted and frozen at -20°C. Individual aliquots were thawed and diluted to the noted concentration in the relevant assay medium.

Microscopy

All imaging was done using an Andor Dragonfly microscope with a Yokugawa spinning disk confocal unit. Samples excited at the indicated wavelength using direct modulation lasers passing through a 405/488/561/640 quad excitation dichroic and imaged with a 60x 1.49 NA Apochromat TIRF objective using a Nikon Eclipse Ti2 inverted microscope. Images were collected using a iXon Life 888 electron-multiplying charge-coupled device camera (Andor). All cells were maintained during imaging in Leibovitz's L15 media without phenol red (Thermo Fisher, 21083027) supplemented with 1% fetal bovine serum (hereafter 'imaging media'). The

microscope is outfitted with a temperature-controlled chamber, and all imaging was conducted at 37˚C.

B2AR internalization was visualized using HEK293 cells stably expressing FLAG-B2AR, passed to PDL-coated 25 mm #1.5 cover slips (Thor Labs, 0117650). Cells were incubated for 10 minutes at 37˚C with 1:2000 M1 mouse anti-FLAG mAb (Sigma Aldrich, F3040) that had been pre-conjugated to Alexa Fluor 647 dye using an Alexa Fluor 647 Protein Labeling Kit (Invitrogen, A20173). Cover slips were then mounted on an imaging chamber in 700 µL imaging media, illuminated with a 637 nm laser, and fluorescence collected through a 700/75 nm bandpass filter. Images were taken every 30 seconds for 1 minute of baseline, then cells treated with isoproterenol in 100 µL imaging media to a final concentration of 10 µM and imaged for 10 minutes of internalization.

For SpH-B2AR internalization and recycling assays, HEK293 cells stably expressing SpH-B2AR were passed to 6-well plates containing PDL-coated 25 mm cover slips and reverse-transfected with 150 ng mCherry-difopein or mCherry-R18 K-mutant negative control peptide for 24 hours. Cover slips were sequentially illuminated with 488 and 561 nm lasers and imaged every 30 seconds for 1 minute of baseline measurements using 540/30 and 600/50 nm bandpass filters, respectively. We then added isoproterenol in 100 µL imaging media to a final concentration of 10 µM and imaged for 10 minutes. We then manually removed the isoproterenol-containing media, replaced it with 800 µL imaging media containing 40 µM alprenolol, and imaged for another 20 minutes. Surface B2AR fluorescence was quantified using an automated macro in ImageJ. We blurred the images using a Gaussian function ($\sigma=1$) to reduce variability, subtracted the background fluorescence from all images, then used automated thresholding to create a mask of the cell membrane in cells expressing both SpH-B2AR and mCherry. We then applied this mask to the background-subtracted images and

11

measured the integrated density of green fluorescence in the resulting regions. Fluorescence is shown as a percentage of the average SpH fluorescence values for the two baseline images.

SILAC sample preparation

SILAC samples were prepared and immunoprecipitated as described previously (Gokhale, Larimore, *et al.*, 2012). HEK293 cells stably expressing FLAG-B2AR were grown in 'heavy' R10K8 or 'light' R0K0 SILAC media for seven passages to allow heavy or light amino acid incorporation into cellular proteins. Each population was then grown to confluence in 10 15-cm dishes. Cells cultured in heavy media were stimulated with 10 µM isoproterenol for 10 minutes to induce internalization, then all samples rinsed three times with cold PBS supplemented with 0.1 M calcium chloride and magnesium chloride (PBS Ca-Mg) and placed on wet ice. Proteins were then crosslinked by incubating with 1 mM DSP in PBS Ca-Mg for 1 hour at 4°C. DSP was quenched by incubating the cells with 25 mM Tris pH 7.4 for 15 minutes on ice. Cells were washed with PBS Ca-Mg and lysed by incubating for 30 minutes in lysis buffer (150 mM NaCl, 10 mM HEPES, 1 mM EGTA, 0.1 $MgCl_2$, 0.5% Triton X-100, supplemented with Complete Antiprotease [Roche, 11245200]), then scraped from the plates. Lysates were spun down at 16,000 g for 15 minutes and the supernatant isolated and diluted to 1 mg/mL protein. 500 µL of lysate was added to 30 µL Dynabeads coated with sheep anti-mouse IgG that had been preloaded with mouse M2 anti-FLAG mAb (Sigma Aldrich, RRID:AB_259529) and incubated on a rotator for 2 hours at 4°C. 340 µM 3xFlag peptide (Sigma Aldrich, F4799) was added to lysates from cells grown in 'light' culture during incubation to outcompete FLAG-B2AR as a negative control. Bound proteins were eluted by incubation in Laemelli sample buffer (Bio-Rad, 1610737) made up to 1x concentration at 75°C for 5 minutes. The eluted lysates wer e pooled and concentrated by trichloroacetic acid precipitation.

Mass spectrometry

Concentrated proteins from FLAG immunoprecipitation were separated on a 4-12% Bis-Tris Novex mini-gel (Invitrogen) using MOPS buffer. 5% of each sample was run on a separate gel and silver stained to visualize total protein isolation. The gel destined for mass spectrometry was stained with Coomassie and excised into forty equal segments using a grid. Gel pieces were processed using a robot (ProGest, DigiLab) to sequentially wash with 25mM ammonium bicarbonate followed by acetonitrile and reduction with 10mM dithiothreitol at 60°C. This was followed by alkylation with 50mM iodoacetamide at room temperature, digestion with trypsin (Promega) at 37°C for 4h, and quenching with formic acid. Supernatant was analyzed directly without further processing. The gel digests were analyzed by nano LC/MS/MS with a Waters NanoAcquity HPLC system interfaced to a ThermoFisher Orbitrap Velos Pro. Peptides were loaded on a trapping column and eluted over a 75 µm analytical column at 350nL/min; both columns were packed with Jupiter Proteo resin (Phenomenex). The mass spectrometer was operated in data-dependent mode, with MS performed in the Orbitrap at 60,000 FWHM resolution and MS/MS performed in the LTQ. The fifteen most abundant ions were selected for MS/MS. Data Processing Data were processed through the MaxQuant software v1.3.0.5 (www.maxquant.org) which was used for recalibration of MS data, filtering of database search results at the 1% protein and peptide false discovery rate (FDR), and calculation of SILAC heavy/light ratios. Data were searched using a local copy of Andromeda with the following parameters: Enzyme = Trypsin; Database = SwissProt Human (concatenated forward and reverse plus common contaminants); Fixed modification = Carbamidomethyl (C); Variable modifications = Oxidation (M), Acetyl (N-term), 13C6/15N2 (K), 13C6/15N4 (R); Fragment Mass Tolerance = 0.5 Da. Pertinent MaxQuant settings were: Peptide FDR = 0.01; Protein FDR = 0.01; Min. peptide Length = 6; Min. unique peptides = 2; Min. ratio count = 2; Re-quantify = TRUE; Keep low-scoring versions of identified peptides = TRUE. Identification of multiprotein complexes was conducted using the MCODE algorithm, with clustering performed based on

13

protein-protein interactions documented by the STRING and BioGRID databases (Bader and Hogue, 2003; Szklarczyk *et al.*, 2019; Oughtred *et al.*, 2021).

FLAG-B2AR co-immunoprecipitation

HEK293 cells stably expressing FLAG-B2AR or a non-expressing, parental HEK293 cell line were seeded in a T75 or T25 flask and transfected with 3 or 1 μg HA-14-3-3ε, respectively, then the transfection-containing media changed after 5 hours. 24-48 hours later, cells were passed to PDL-coated 10 cm dishes, with FLAG-B2AR cells split into two plates, and incubated for 24 hours. FLAG-B2AR dishes were treated with either 10 μM isoproterenol or an H_2O vehicle control and incubated for 10 minutes at 37˚C, while the HEK293 control dish was treated with H_2O vehicle. Cells were then placed on ice, washed twice with cold PBS, treated with 500 μL immunoprecipitation lysis buffer (as described for SILAC co-IP above), lifted using a cell scraper, and lysed by pipetting. Lysates were centrifuged at 13,200 g for 15 minutes at 4˚C and the supernatant isolated. Protein concentration was measured using a BCA assay (Thermo Fisher Scientific, 23225) and all lysates made up to equivalent concentrations using lysis buffer. 0.75-1 mg of lysate was incubated for 1 hour at room temperature with Sheep anti-mouse IgG Dynabeads preloaded with M2 anti-FLAG mouse mAb. Beads were then washed six times with cold IP buffer (150 mM NaCl, 10 mM HEPES, 1 mM EGTA, 0.1 $MgCl_2$) using a magnetic rack, then eluted at 95˚C for 10 minutes in 30 μL reducing sample buffer (RSB): 2x Laemmli sample buffer made up to a final concentration of 1x with nanopure H_2O and supplemented with protease inhibitors (1 minitablet dissolved in 1 mL H_2O, made up to 1x; Thermo Fisher Scientific, A32965), phosphatase inhibitors (1 minitablet dissolved in 1 mL H_2O, made up to 1x; Thermo Fisher Scientific, A32957), DL-dithiothreitol (50 mM final concentration; Sigma Aldrich, D9779) and 10% 2-mercaptoethanol (Bio-Rad, 1610710). Enough cell lysate to equal 2% of the amount of total protein loaded onto the beads was made up to 30 μL in RSB and incubated at 95˚C for 10 minutes.

14

Immunoblotting

For FLAG-B2AR co-immunoprecipitation immunoblotting, 30 µL each of elutes and 2% inputs were run out on precast 10-well 4-20% BioRad miniProtean gels (4560194) and transferred to nitrocellulose membranes. Membranes were blocked with 5% weight by volume milk (Research Products International, M17200-500) in Tris-buffered saline with 0.1% Tween (TBST; Thermo Fisher Scientific, BP337-500) and labeled with 1:1000 HA-tag rabbit mAb (Cell Signaling Technology, RRID:AB_1549585) followed by 1:5000 goat anti-rabbit HRP (Bio-Rad, 1706515). We then incubated the membranes with SuperSignal West Dura Chemiluminescent Substrate (Thermo Fisher Scientific, 34075) for 5 minutes and imaged chemiluminescence using an Invitrogen iBright FL1000. Membranes were then stripped using Restore Western Blot Stripping Buffer (Thermo Fisher Scientific 21059) for 30 minutes, reblocked in milk in TBST, labeled with 1:2000 M2 anti-FLAG followed by 1:5000 goat anti-mouse HRP (Bio-Rad, 170-6516), then developed and imaged as previously. We calculated densitometry using ImageJ.

For blots assessing ERK phosphorylation, HEK293 cells stably expressing FLAG-B2AR were reverse transfected with 150 ng of the described plasmids in PDL-coated 12 well plates and let settle overnight. The following day, cells were starved for 4 hours in serum-free DMEM to decrease basal ERK phosphorylation. Wells were incubated with 10 µM isoproterenol for the reported time, then washed twice with cold PBS and lysed in Laemmli sample buffer supplemented with protease inhibitors, phosphatase inhibitors, and 10% 2-mercaptoethanol. We then added DL-dithiothreitol to a final concentration of 25 mM and incubated lysates at 95°C for 10 minutes. Lysates were run on 12-well 4-20% BioRad miniProtean gels (4560195) and transferred to nitrocellulose membranes. For measuring phosphorylated ERK, membranes were blocked in 5% weight by volume BSA (Thermo Fisher Scientific, BP1600-100) in TBST to avoid dephosphorylation by phosphatases present in milk and labeled with 1:1000 rabbit phospho-

15

MAPK Y202/Y204 mAb (Cell Signaling Technology, RRID:AB_331772). All imaging conditions were the same as above, except chemiluminescence was developed using SuperSignal West Pico Chemiluminescent Substrate (Thermo Fisher Scientific, 34580) due the higher expected signal. Total ERK was probed using with 1:1000 mouse p44/42 MAPK mAb (Cell Signaling Technology, 4696). Data are presented as the band density of phosphorylated ERK divided by that of total ERK as a percentage of the peak value for cells expressing YFP-R18 K-mutant.

APEX proximity labeling

Proximity labeling with APEX2 was conducted as has been described previously (Hung *et al.*, 2016), with minor modifications. HEK293 cells stably expressing FLAG-B2AR-APEX were plated in 6-well plates coated with PDL and let grow to 90% confluence. Biotin phenol (Sigma-Aldrich, SML2135) was added to cells as a 100x concentrated stock in DMSO (or an equivalent volume of DMSO vehicle) to a final concentration of 50 µM and the plates incubated for 30 minutes at 37˚C. We then added 100 mM hydrogen peroxide in water to a final concentration of 1 mM (or water vehicle), incubated the plates for 1 minute at room temperature, then aspirated the media and replaced with a reaction quenching buffer (Dulbecco's PBS supplemented with 10 mM sodium ascorbate [Sigma-Aldrich, A4034], 5 mM Trolox [Sigma-Aldrich, 238813], and 10 mM sodium azide [Thermo Fisher Scientific, BP922I]). Cells were washed twice more with quenching buffer, then scraped from the plates and transferred into centrifuge tubes and spun down to pellet cells. Cell pellets were lysed in RIPA buffer (Thermo Fisher Scientific, 89900) supplemented with protease inhibitors (1 minitablet dissolved in 1 mL H_2O, made up to 1x; Thermo Fisher Scientific, A32965), 10 mM sodium ascorbate, 5 mM Trolox, and 10 mM sodium azide (hereafter 'lysis buffer'), then clarified via centrifugation. We measured protein concentration using the Pierce 660 assay and made up all lysates for a given experiment to equal concentrations.

Cell lysates were rotated for one hour at room temperature or overnight at 4°C with Pierce magnetic streptavidin beads (Thermo Fisher Scientific, 88816) that had been blocked in 0.1% bovine serum albumin for one hour at room temperature. Beads were washed twice with RIPA buffer, once with 1 M KCl (EMD, PX1405), once with 0.1 M Na_2CO_3 (Sigma Aldrich, S5761) once with 2 M urea (Thermo Fisher Scientific, U15) in 10 mM Tris base (Avantor, 4099-06) made up to pH 8.0 using HCl, and twice again with RIPA buffer, all kept cold on wet ice. Lysates were eluted by incubating in Laemmli sample buffer (Bio-Rad, 1610737) made up to 3x concentration with water and supplemented with 2 mM biotin (Sigma-Aldrich, B4501) and 20 mM DL-dithiothreitol (DTT; Sigma Aldrich, D9779) for 10 minutes at 95°C. Immunoblotting was conducted as described above except that membranes were blocked by incubation for 1 hour at room temperature in Intercept (TBS) Blocking Buffer (LI-COR Biosciences, 927-60001), then biotinylated proteins labeled with 1:1000 IRdye 800CW Streptavidin (LI-COR, 926-32230) in Intercept buffer for 1 hour at room temperature while protected from light. Biotinylation was imaged using the infrared fluorescence detection mode on an Invitrogen iBright FL1000.

NanoBit

NanoBit protein-protein interaction assays were performed in 96-well, solid bottom white plates coated with poly-D-lysine. 6×10^4 HEK293 cells were passed to each well and reverse transfected for 24 hours with 10 ng of each noted plasmid, unless otherwise noted. Wells were washed twice with PBS, then incubated for 10 minutes with 10 μM furimazine in 100 μL Leibovitz's L-15 media supplemented with 1% FBS at 37°C. NanoBit luminescence was measured on a Varioskan LUX multimode microplate reader once every one minute for ten minutes, then the plate was removed, treatment added, and readings taken again for 30 or 60 minutes. All traces were normalized to the average baseline value, then corrected for substrate decay by fitting an exponential curve to the vehicle-treated condition and multiplying all curves by the inverse of the resulting function.

AlphaFold Multimer structural predictions

AlphaFold Multimer was used to predict the structure of full-length B2AR in complex with full length 14-3-3ε and 14-3-3ζ/δ. AlphaFold Multimer has been previously described and was used without modification through the gateway COSMIC2 (Cianfrocco *et al.*, 2017; Evans *et al.*, 2022). Five models were developed with the following parameters: db_preset_ = full_dbs, max_template_date = 2023-05-30, model_preset_ = multimer, model_to_relax_ = none, num_multimer_predictions_per_model_ = 1. All data shown is from the first, highest-ranked model. Structures were visualized and annotated using UCSF ChimeraX (Pettersen *et al.*, 2021). The first 20 amino acids of the B2AR N-terminus were removed from visualization for spatial concision, but were included in structural predictions and do not interact with 14-3-3 proteins in this model.

cAMP GloSensor

Cyclic AMP in live HEK293 cells was measured using the luminescent cAMP sensor Promega cAMP GloSensor 22F. Luminescence measurements were performed in 96-well, solid bottom white plates (Costar Corning, 3917) coated with poly-D-lysine to promote cell adherence (Sigma Aldrich, #P6407). $5x10^4$ HEK293 cells were passed to each well and reverse transfected for 24 hours with 20 ng each of cAMP GloSensor and any noted test plasmids. Cells were washed twice with PBS, then incubated for 2 hours with 500 μg/mL D-luciferin (Goldbio, LUCK-1G) in 100 μL Leibovitz's L-15 media supplemented with 10% fetal bovine serum at room temperature. Luminescence was measured on a Varioskan LUX multimode microplate reader at either 250 or 500 ms exposure time once per minute for ten minutes, the plate was removed, treatment added, then readings taken again once per minute for one hour. All treatments were diluted to 10-fold concentrated stocks in Leibovitz's L-15 media supplemented with 10% FBS at

18

room temperature and added to the final concentration described. Traces were normalized to the average value prior to treatment and then represented as a percent of the peak value for the R18 K-mutant negative control peptide or empty vector transfected condition at 10 µM treatment.

Statistics and figure production

All statistics were performed and data graphs produced using GraphPad Prism 10, except for gene ontology analysis. Due to the exploratory nature of this study, all statistical tests represent a description of the data presented, rather than a test of a hypothesis formulated prior to the commencement of the investigation. Experiments comparing two means were analyzed using a two-tailed Student's t-test, while those comparing three or more means were analyzed using a one-way analysis of variance (ANOVA), with Dunnet's multiple comparisons test where individual comparisons were made. These tests were conducted with pairing when individual data points were produced from the same immunoblot or assay plate. Concentration-response curves were fit to a three-parameter nonlinear regression. The resulting curves were analyzed using an extra sum-of-squares F-test, comparing the bottom, top, and logEC50 of the individual curves to a global fit model to determine whether the curves are best fit by a single model or by multiple, different fits. Gene ontology analysis (Ashburner *et al.*, 2000; The Gene Ontology Consortium *et al.*, 2023) was conducted and graphs produced using WebGestalt (Liao *et al.*, 2019) with the following parameters: Enrichment method = ORA, Enrichment categories = geneontology_Biological_Process_noRedundant, Reference Set = genome, IDtype = genesymbol, Minimum IDs/category = 5, Maximum IDs/category = 2000, FDR method = BH, Significance level = top 10. Experimental schematic and model figure panels were created with BioRender.com. All figures were produced using Adobe Illustrator 28.0.

19

Results

SILAC-based immunoprecipitation identifies the B2AR interactome with high fidelity.

To identify the stable interactome of agonist-stimulated B2AR, composed of direct and indirect interactors of the receptor, we opted to use immunoprecipitation of B2AR tagged with an N-terminal FLAG epitope (FLAG-B2AR) expressed in HEK293 cells. This engineered receptor has the key advantage of leaving the intracellular domains of B2AR unmodified. We and others have extensively characterized the trafficking, signaling, and biochemical characteristics of this tagged B2AR (Cao *et al.*, 1999; Lauffer *et al.*, 2010; Puthenveedu *et al.*, 2010; Irannejad *et al.*, 2013). Consistent with previous data, live imaging of surface FLAG-B2AR with an M1 anti-FLAG antibody conjugated to Alexa Fluor 647 (M1-647) showed agonist-mediated internalization upon addition of 10 µM isoproterenol and localized primarily at endosomes within ten minutes (Fig. 1A). To minimize variability between experimental conditions during the mass spectrometry process and allow direct, quantitative comparison between samples, we opted to use a SILAC-based approach comparing the agonist-stimulated B2AR interactome with a negative control sample to filter out non-specific proteins. This experimental protocol has previously been used to identify protein interactomes with high fidelity (Gokhale, Perez-Cornejo, *et al.*, 2012; Perez-Cornejo *et al.*, 2012; Ryder *et al.*, 2013a; b; Gokhale *et al.*, 2016). HEK293 cells stably expressing FLAG-B2AR were grown in media containing either arginine and lysine with "light" 12C and 14N (R0K0) or "heavy" 13C and 15N (R10K8) for more than six passages to ensure equilibrium labeling of the proteome. Using this method, we can reliably achieve steady labeling of >98% of the proteome with R10K8 in HEK293 cells (Gokhale, Larimore, *et al.*, 2012; Perez-Cornejo *et al.*, 2012). We used "light" labeled cells as our negative control condition and "heavy" labeled cells as our ligand-stimulated B2AR immunoprecipitation condition.

20

HEK293 FLAG-B2AR cells labeled with "heavy" isotopes were treated with 10 μM isoproterenol for 10 minutes to induce internalization, then both experimental and negative control cells placed on ice to stop further trafficking and incubated with DSP to cross-link B2AR with associated proteins. We opted to crosslink to ensure that we capture the a greater proportion of larger, multi-subunit complexes where not all components might directly bind to the receptor (Gokhale, Perez-Cornejo, *et al.*, 2012; Perez-Cornejo *et al.*, 2012; Ryder *et al.*, 2013b; Gokhale *et al.*, 2016). We isolated FLAG-B2AR and interacting proteins using Dynabead magnetic beads conjugated to sheep anti-mouse IgG and incubated with mouse M2 anti-FLAG antibodies. As a negative control, samples labeled with "light" isotopes were incubated with an excess of FLAG peptide to outcompete FLAG-B2AR binding. This control identified proteins that nonspecifically bound the magnetic beads. Silver stained SDS page of whole-cell lysate and anti-FLAG immunoprecipitated proteins shows isolation of a small subset of the total proteins present (Fig. 1B). Pooled FLAG-B2AR and negative control samples were analyzed using mass spectrometry.

We used fold enrichment and the number of peptides detected as criteria to identify proteins associated with ligand-activated B2AR. We identified 190 proteins (not including B2AR itself) in pooled samples that were enriched at least two fold in the stimulated FLAG-B2AR immunoprecipitation condition over the excess FLAG peptide negative control and after curation with a library of proteins that spuriously interact with FLAG antibody-coated magnetic beads (Fig. 1C-D). The B2AR interactome is enriched in proteins annotated to membrane trafficking terms (Fig. 2A). For example, the B2AR interactome was enriched more than 10-fold in proteins annotated to the gene ontology (GO) term 'endosomal transport' ($q < 2.2 \times 10^{-16}$, GO: 0016197) and more than 9-fold in proteins annotated to the GO term 'membrane fusion' ($q < 3.45 \times 10^{-9}$, GO: 0061025; Fig. 2A, Supplementary Table 1, Extended Data 1). Among the proteins belonging to these ontological terms, we found most known B2AR binding partners and proteins

21

previously shown to associate with B2AR throughout the receptor trafficking itinerary. These proteins include beta arrestin 2, clathrin heavy and light chains, and accessory protein 2 subunits alpha, beta, and mu, which are all essential elements of the B2AR internalization machinery and enriched at least 4-fold over the negative control (Wolfe and Trejo, 2007). Also present and highly enriched (8- to 15-fold over negative control) are well-characterized B2AR-binding proteins such as NSF and the PDZ domain-containing proteins NHERF1, NHERF2, and SNX27 (Hall *et al.*, 1998; Cong *et al.*, 2001; He *et al.*, 2006; Lauffer *et al.*, 2010). All Retromer core components (VPS26A/B, VPS29 and VPS35) and three of five members of the WASP and SCAR Homologue (WASH) complex (WASHC2/FAM21A, WASHC4/KIAA1033, and WASHC5/strumpellin), which interact with the PDZ-domain proteins, were likewise detectable and at least 4-fold enriched (Fig. 1D, Extended Data 2) (Gomez and Billadeau, 2009; Varandas *et al.*, 2016). Proteins with previously-described roles in endosomal sorting and cargo recycling, including EEA1, Rab5, Rab11 (5- to 10-fold), and cortactin (2.6-fold), were also enriched in this pool (Ullrich *et al.*, 1996; Christoforidis *et al.*, 1999; Moore *et al.*, 2004; Puthenveedu *et al.*, 2010; Zeigerer *et al.*, 2012; Vistein and Puthenveedu, 2014). These data show that our approach was able to identify, with high confidence, members of large protein complexes that interact with B2AR. We also identified many members of the CORVET and CCC complexes, which are both known to play roles in endosomal cargo sorting, but which have not previously been shown to interact with B2AR (Beek *et al.*, 2019; Singla *et al.*, 2019; Boesch *et al.*, 2023). Clustering using the Molecular Complex Detection (MCODE) algorithm based on previously-reported protein-protein interactions compiled in the STRING and BioGRID databases revealed identified multiple complexes involved in endosomal cargo sorting, including WASH, CORVET, and the CCC-Retriever complexes (Fig. 2B) (Bader and Hogue, 2003; Szklarczyk *et al.*, 2019; Oughtred *et al.*, 2021). Overall, we determined via literature search that 16 of the 190 proteins identified as part of the B2AR cross-linked interactome (8.4%) have been reported previously to bind B2AR directly, while a further 39 (20.5%) are known to form complexes with direct B2AR

binding partners or colocalize closely with the receptor in fluorescence microscopy (Extended Data 2). These include several proteins for which association with B2AR has been reported, but for which little is known about their functional role in receptor activity (Karoor *et al.*, 1998; Maïssa *et al.*, 2017; Pons *et al.*, 2017).

B2AR binds to 14-3-3 proteins in the absence of agonist stimulation.

We focused on the 14-3-3 family of proteins to follow up on functionally, as they have been shown to play numerous roles in regulating intracellular signaling pathways (Masters and Fu, 2001; Tutor *et al.*, 2006; Thompson and Goldspink, 2022; Yang *et al.*, 2023). We identified six of the seven human 14-3-3 protein isoforms enriched at least 3-fold over the negative control condition, with the most enriched isoforms (14-3-3ε, ζ/δ, and θ) enriched more than 5-fold. This enrichment is within the range of subunits of the WASH complex and the adaptor complex AP-2, both well-established interactors of B2AR (4.5- to 8-fold enrichment). The only isoform not detected was sigma, which is expressed only at very low levels or not at all in HEK293 cells. 14-3-3σ (gene name SFN) mRNA has been reported at only 5.0 transcripts per million, compared to 873.8 for *YWHAE*, the gene encoding 14-3-3ε (Uhlén *et al.*, 2015; Cell line - SFN - The Human Protein Atlas, n.d.; Cell line - YWHAE - The Human Protein Atlas, n.d.). On a protein level, 14-3-3 proteins other than 14-3-3σ are generally expressed at high levels in HEK293, with intracellular concentrations ranging from 3 μM for 14-3-3η to 14 μM for 14-3-3ε, and displaying a broadly cytoplasmic localization (Cho *et al.*, 2022). 14-3-3 proteins are a versatile class of scaffolding proteins that have been previously reported to associate with various G protein-coupled receptors, including B2AR (Tazawa *et al.*, 2003; Tutor *et al.*, 2006; Grant *et al.*, 2011; Li *et al.*, 2016; Yuan *et al.*, 2019), but how 14-3-3 proteins regulate receptor signaling and trafficking have not been well characterized.

23

To confirm our proteomics data and to test whether 14-3-3 interactions were agonist-regulated, we first sought to identify 14-3-3 protein association with FLAG-B2AR by immunoprecipitation and direct detection. When B2AR was immuno-isolated with an anti-FLAG antibody in HEK293 cells stably expressing FLAG-B2AR and transfected with HA-14-3-3ε (the most abundant 14-3-3 isoform in our SILAC co-IP with 13 total spectra, alongside 14-3-3ζ/δ with an equal number), 14-3-3ε was isolated along with B2AR, confirming that B2AR associated with 14-3-3ε (Fig. 3A). This association was observed in the absence of cross-linking agents in this experiment, indicating that the B2AR-14-3-3 complex is capable of surviving cell lysis and stringent washes during immunoprecipitation. As a negative control, an identical protocol in the parental HEK293 cell line not expressing FLAG-B2AR did not pull down 14-3-3ε (Fig. 3A-B). Treatment with isoproterenol decreased mean HA-14-3-3ε association with FLAG-B2AR by more than 50%. FLAG-B2AR cells treated with 10 μM iso for 10 minutes showed an average of 41.21% of the amount of HA-14-3-3ε pulled down by the same cells treated with an H_2O vehicle (95% confidence interval: -4.42-86.84%). We also observed a decrease in FLAG immunolabeling in cells treated with iso following immunoprecipitation, possibly due to impaired solubilization of the receptor after internalization. However, this decrease was smaller than the decline seen in HA-14-3-3ε pulldown, indicating that the reduced FLAG-B2AR isolation does not fully explain the decreased amount of 14-3-3ε.

We used proximity labeling with APEX2 and NanoBit-based luciferase complementation as orthogonal methods for establishing agonist-dependence of B2AR interactions with 14-3-3 proteins that does not rely on receptor immunoisolation. APEX is an engineered ascorbic acid peroxidase that produces reactive biotin phenol radicals when activated with hydrogen peroxide. These radicals irreversibly biotinylate adjacent proteins, allowing the isolation and identification of the local protein environment. We inserted APEX2 into the B2AR C-terminal tail after proline 382. This construct (B2AR-APEX) was modeled off one that has been used previously to

24

investigate the B2AR interactome (Lobingier *et al.*, 2017). B2AR-APEX is expressed at the plasma membrane in HEK293 cells and internalizes in response to stimulation with isoproterenol (Supplementary Fig. 1A). HEK293 cells stably expressing B2AR-APEX show a substantial increase in biotinylation upon APEX activation with hydrogen peroxide, and biotinylated proteins can be isolated using streptavidin beads (Supplementary Fig. 1B). Overexpressed HA-14-3-3ε in B2AR-APEX cells is biotinylated in response to APEX activation, with reduced biotinylation apparent when cells were pretreated with isoproterenol (Fig. 3D). We then employed a NanoBit assay, using B2AR with the Large Bit (LgBit) inserted at the same site in the receptor C-terminal tail as used for APEX and 14-3-3 protein tagged on the N terminus with Small Bit (SmBit) (Fig. 3E). Transfection of HEK293 cells with B2AR-LgBit and increasing amounts of SmBit-14-3-3ε results in increased basal luminescence compared to expression of B2AR-LgBit alone, supporting the conclusion that these proteins associate prior to receptor stimulation (Fig. 3F). Stimulation of B2AR with isoproterenol results in a general trend towards decreased luminescence–consistent with dissociation of 14-3-3 proteins from B2AR after receptor activation–although occurring over a longer time period using this assay and not reaching statistical significance (Fig. 3G).

Seeking to determine whether 14-3-3 is likely to bind B2AR directly and–if so–identify specific, structural information about this association, we used Alphafold Multimer to predict the structure of B2AR bound to a dimer composed of 14-3-3ε and ζ/δ. AlphaFold is a machine learning-based method for predicting protein structure; AlphaFold-Multimer extends these predictions to multi-protein complexes (Jumper *et al.*, 2021; Evans *et al.*, 2022). We chose the ε and ζ/δ isoforms as these were the two most abundant in our SILAC co-IP. 14-3-3 proteins can act as both homo- or heterodimers, but the ε isoform preferentially forms heterodimers, making this combination a likely candidate for specific association with B2AR (Chaudhri *et al.*, 2003; Yang *et al.*, 2006).

25

The top five predicted structures each showed association between the intracellular domains of B2AR and the canonical 14-3-3 protein substrate binding sites (Fig. 3H). All predicted B2AR ICL3 insertion into one 14-3-3 binding groove, with the other occupied by the receiver's distal C-terminus (Fig. 3H, Supplementary Fig. 2A-B). The transmembrane regions of B2AR showed an average predicted local distance difference test (pLDDT) score of 89.0 for the top structural model, scoring these domains as well-modeled (Fig. 3I) (Mariani *et al.*, 2013; Tunyasuvunakool *et al.*, 2021). Non-transmembrane regions were modeled with lower confidence, with a mean pLDDT score of just 39.7, consistent with previous structural information indicating that the B2AR termini and intracellular loop 3 are largely disordered (Heng *et al.*, 2023). 14-3-3 proteins were generally well-modeled, with average pLDDT scores of 87.9 and 91.2 for 14-3-3ε and ζ/δ, respectively. Both showed good predicted accuracy around the canonical binding sites–with pLDDT for all sites greater than 90–and low confidence predictions only at the distal termini, especially the C-terminus, which is not involved in substrate binding (Yang *et al.*, 2006).

14-3-3 proteins regulate cAMP production downstream of B2AR activation

We first wanted to ask whether 14-3-3 proteins play a previously-undiscovered role in regulating second messenger signaling following B2AR activation. If our AlphaFold structural prediction is correct, and unstimulated B2AR does bind to 14-3-3 proteins via engagement of both the third intracellular loop and C-terminus, we would expect that 14-3-3 proteins would sterically block association with immediate signaling effectors. We began testing this hypothesis first by investigating cyclic AMP (cAMP) signaling activated by B2AR stimulation of Gαs. To measure total cAMP production and signaling dynamics in live cells, we transiently transfected HEK293 cells with pGloSensor 22F (hereafter GloSensor), a genetically-encoded,

bioluminescence-based cAMP sensor. GloSensor is composed of a circularly-permutated firefly

luciferase into which a protein kinase A (PKA) regulatory domain has been inserted (Binkowski

et al., 2011). cAMP binding to this regulatory domain induces a conformational change that

increases luminescence when incubated with the substrate luciferin.

We used YFP-difopein, a peptide inhibitor of 14-3-3 proteins, to determine the role of 14-3-3

proteins in regulating B2AR signaling. Difopein is composed of two consecutive R18 peptide

segments, derived from the 14-3-3 binding motif of Raf-1, separated by a short linker region.

Unlike the parent Raf-1 motif, R18 does not need to be phosphorylated to bind and inhibit 14-3-

3 proteins due to the replacement of serine residues with negatively-charged aspartic and

glutamic acid. We used a YFP-R18 peptide with these phosphomimetic residues mutated to

positively charged lysines (R18 K-mut) as a negative control. This charge-swapping mutation

abolishes R18 binding to 14-3-3 proteins (Masters and Fu, 2001).

HEK293 cells endogenously express B2AR and initiate cAMP production when treated with

isoproterenol (Tsvetanova and von Zastrow, 2014). Total cAMP production was defined as the

area under the curve (AUC) of the luminescence traces for the first 30 minutes after agonist

addition; data are shown as a percentage of the 10 µM isoproterenol treatment condition for

cells transfected with the R18 K-mut negative control peptide. cAMP production followed a

standard, sigmoidal concentration-response curve, albeit with a small decrease at

supersaturating isoproterenol concentrations (above 1 µM; Fig. 4A-B).

Transfecting HEK293 cells with difopein resulted in substantially greater total cAMP

production after stimulation with isoproterenol when compared to transfection with the R18 K-

mut negative control peptide (Fig. 4A-B). A concentration-response curve fit to the mean total

cAMP production of cells transfected with difopein resulted in a non-linear model with a

27

response plateau at 329.6% (95 percent confidence interval: 255.8-406.9%) of the average

cAMP production after treatment with 10 µM iso for cells transfected with R18 K-mut (Fig. 4B).

There was no statistically significant difference in EC50 between parameters derived from best-

fit curves fit to cells expressing R18 K-mut (EC50=9.063 nM, 95 percent confidence interval:

4.554-17.52 nM) and those expressing difopein (EC50=9.647 nM, 95 percent confidence

interval: 1.779-45.38 nM). 14-3-3 proteins are versatile scaffolds with a large number of

substrates (Aghazadeh and Papadopoulos, 2016; Pennington *et al.*, 2018). As such, we wished

to see whether their impact on cAMP signaling in this system is entirely due to their interaction

with B2AR, or whether they may play roles at multiple points in this pathway. Total cAMP

production in response to direct adenylyl cyclase activation with forskolin was also enhanced by

14-3-3 inhibition with difopein (Fig. 4C). HEK293 cells transiently transfected with GloSensor

and difopein showed a mean total cAMP production of 208.0% (95% confidence interval: 107.9-

308.2%) of the response in cells transfected with the negative control peptide after stimulation

with 10 µM forskolin (Fig. 4D). The mean raw luminescence AUC values and 95% confidence

intervals for cells expressing the control peptide were comparable upon treatment with 10 µM of

either isoproterenol or forskolin (7284560 ± 448705 and 772759 ± 517868 arbitrary

luminescence units for iso and forskolin respectively), showing that the effect was not due to

differences in cAMP generated by the two treatments. As 14-3-3 binds to phosphodiesterases

and protects them from dephosphorylation and inactivation (Pozuelo Rubio *et al.*, 2005; Palmer

et al., 2007; Vandeput *et al.*, 2013), this may indicate that B2AR forms macromolecular

signaling complexes that include 14-3-3 proteins and phosphodiesterases (Fraser *et al.*, 2000;

Perry *et al.*, 2002; Bauman *et al.*, 2006).

While some portion of the impact of 14-3-3 proteins on B2AR-initiated cAMP signaling may

be due to effects downstream of adenylyl cyclase activation, we sought to determine whether

there exists also a proximal impact on G protein recruitment to the receptor using a NanoBit

28

luciferase complementation assay (Fig. 5A). The reconstituted NanoBit dimer has a peak emission wavelength of 460 nm (Dixon *et al.*, 2016). This is similar to the parent NanoLuc protein, which can form a BRET pair with YFP (Besson *et al.*, 2022). To avoid any spectral complications from co-expression of these proteins, we replaced the YFP on our YFP-difopein and negative control plasmids with mCherry. These plasmids produced a similar result to our YFP-tagged versions when tested in the cAMP GloSensor assay, with a greater increase in total mean cAMP apparent upon B2AR stimulation when expressing mCherry-difopein compared to the negative control (Supplementary Fig. 3). Coexpression of B2AR-LgBit with SmBit-miniGs and stimulation with isoproterenol results in a rapid increase in luminescence, indicative of miniGs recruitment to the receptor, followed by sustained signal without obvious miniGs dissociation from B2AR (Fig. 5B). 14-3-3 inhibition with mCherry-difopein increases SmBit-miniGs recruitment to the receptor compared to expression of the mCherry-tagged control peptide, as shown by fitting of concentration-response curves to the peak luminescence values after isoproterenol treatment (Fig. 5C). The response plateau for cells expressing difopein was significantly greater (379.2% of peak luminescence in the control peptide condition treated with 10 µM isoproterenol, 95% confidence interval: 310.2-454.0%) than in cells expressing the control peptide (110.8% of the 10 µM isoproterenol peak, 95% confidence interval: 104.1-117.6%). There was no difference in the EC50 values when 14-3-3 proteins were inhibited (37.0 nM, 95% confidence interval: 7.24-164.3 nM) compared to the control condition (32.1 nM, 95% confidence interval: 18.2-56.0 nM), consistent with the lack of any change in isoproterenol potency in cAMP signaling. The increase in peak miniGs recruitment was also accompanied by an increase in basal association, as indicated by an increase in luminescence prior to treatment from 22.69% of the control peptide condition peak at 10 µM for cells expressing the control peptide (95% confidence interval: 14.38-31.00%) to 66.13% for cells expressing difopein (95% confidence interval: 35.92-96.34%; Fig. 5D).

Overexpressing HA-14-3-3ε did not impact total cAMP production upon stimulation with isoproterenol compared to transfections with an empty vector control (Supplementary Fig. 4A-B). This was true with respect to both maximum cAMP response (AUC concentration-response plateau of 121.5% of empty vector AUC at 10 µM, 95% confidence interval: 111.0-132.2%) and EC50 (8.272 nM, 95% confidence interval: 4.443-14.97 nM) compared to the empty vector (concentration-response plateau=112.3% of AUC at 10 µM, 95% confidence interval: 105.0-119.8%; EC50=10.72 nM, 95% confidence interval: 6.813-16.79 nM) when analyzing parameters produced by fitting the mean AUC values for each condition to a three-parameter non-linear regression. Similarly, there was no clear effect of overexpressing 14-3-3ε on miniGs recruitment to B2AR, as measured by the NanoBit assay (Supplementary Fig. 4C). We hypothesize that this is due to the high endogenous expression of 14-3-3 proteins saturating their impact on cAMP signaling.

14-3-3 proteins regulate arrestin recruitment to activated B2AR

After showing that 14-3-3 proteins regulate the magnitude of B2AR signaling via cAMP and impair G protein recruitment to the receptor, we hypothesized that 14-3-3 proteins act by altering the amount of the receptor available to engage with protein partners. Alongside G proteins, arrestins are the second major class of effectors through with B2AR can act, with recruitment leading to receptor internalization and possibly contributing to initiation of signaling cascades (Kahsai *et al.*, 2023). We used a NanoBit assay to determine whether 14-3-3 proteins impact arrestin recruitment to B2AR, co-expressing B2AR-LgBit with a β-arrestin 2 construct tagged with SmBit on the C-terminus (β arrestin 2-SmBit; Fig. 6A). β-arrestin 2-SmBit is rapidly recruited to B2AR-LgBit after receptor stimulation with isoproterenol, as shown by an increase in total luminescence (Fig. 5B). This response peaks at two minutes post-agonist, then declines to a plateau above the baseline value.

30

Inhibiting 14-3-3 proteins by overexpressing mCherry-difopein increases β-arrestin 2-SmBit recruitment to B2AR-LgBit compared to a negative control peptide (Fig. 6B-C). Arrestin recruitment to B2AR-LgBit cells transfected with mCherry-difopein follows a similar time-course to those expressing the negative control peptide, but with a statistically significantly higher peak luminescence signal of 194% of the negative control peak (95 percent confidence interval: 172.9-217.1%), when comparing best-fit parameters of a three-parameter non-linear regression fit to the mean peak luminescence signal across concentrations of isoproterenol. 14-3-3 inhibition also lead to a statistically significant increase in mean baseline arrestin-B2AR NanoBit signal, with a basal luminescence of 44.67% of the negative control post-agonist peak in mCherry-difopein overexpressing cells (95 percent confidence interval: 22.29-67.04%), compared to 20.26% of the peak in cells transfected with the negative control peptide (95 percent confidence interval: 10.26-30.26%; Fig. 6D). There was no statistically significant difference between the concentration of isoproterenol necessary to recruit arrestin to B2AR in cells overexpressing the 14-3-3 inhibitory peptide (EC50=73.5 nM, 95 percent confidence interval: 28.12-177.6 nM) and those overexpressing the negative control peptide (EC50=77.65 nM, 95 percent confidence interval: 12.07-120.7 nM). We conclude that 14-3-3 proteins impair both agonist-stimulated arrestin recruitment and basal arrestin association with the receptor. Similar to the role of 14-3-3 proteins in regulating cAMP signaling, this acts by increasing the total response, rather than shifting the receptor's sensitivity to agonist.

14-3-3 proteins do not regulate ERK activation downstream of B2AR or receptor trafficking

In addition to initiating cAMP production, B2AR stimulation promotes activation of the MAP kinase cascade, including ERK1/2. The signaling pathways responsible are not entirely clear, with studies variously attributing B2AR-mediated ERK activation to action through Gαs, Gβγ, and beta arrestins, and originating from either the plasma membrane or the endosome (O'Hayre *et al.*, 2017; Luttrell *et al.*, 2018; Kwon *et al.*, 2022). Having seen that 14-3-3 proteins act as negative regulators of both G protein and arrestin recruitment, we wanted to determine whether 14-3-3 proteins additional effects on signaling through the MAP kinase pathway as well.

We treated HEK293 cells stably overexpressing FLAG-B2AR with 10 μM isoproterenol for 2, 5, 10, 15, or 20 minutes, then assessed ERK phosphorylation using Western blot with phospho-specific antibodies. Previous reports have demonstrated that B2AR stimulation with isoproterenol causes a rapid increase in ERK phosphorylation which then declines to a plateau (O'Hayre *et al.*, 2017). Our findings were consistent with this literature. HEK293 cells expressing FLAG-B2AR and transfected with the negative control peptide show a peak in ERK phosphorylation two minutes after stimulation with 10 μM isoproterenol, with the mean ratio of phosphorylated to total ERK reaching approximately ten times the basal level (Fig. 7A-B; baseline pERK/ERK ratio of 10.115% of the peak response, 95% confidence interval: 5.405-14.825). ERK phosphorylation then declined to an average plateau of approximately 30% of the maximum value (30.507% of the mean peak value at 20 minutes, 95% confidence interval: 20.733-40.280). Inhibiting 14-3-3 proteins produced no change in either the magnitude nor dynamics of ERK phosphorylation. Cells transfected with difopein showed mean maximal ERK phosphorylation of 107.941% of the negative control maximum (95% confidence interval: 63.736-152.147) at 2 minutes post-isoproterenol treatment (Fig. 7C). There was no statistically significant difference in mean peak phosphorylated to total ERK ratio in cells expressing difopein when compared to the negative control peptide. Based on these data we conclude that,

despite regulating cAMP production after B2AR stimulation, 14-3-3 proteins do not have a comparable effect on B2AR-initiated ERK signaling.

Alongside possibly regulating ERK phosphorylation, arrestin's major role in B2AR function is to promote receptor endocytosis. As such, we wanted to see whether the impact of 14-3-3 proteins on arrestin recruitment leads to alteration in bulk B2AR trafficking. To quantify B2AR internalization and surface recycling in the presence of 14-3-3 inhibition, we used HEK293 cells stably expressing B2AR conjugated on the N-terminus to supereclliptic pHluorin (SpH), a pH-sensitive version of GFP. This SpH-B2AR construct fluoresces when present at the plasma membrane and SpH is exposed to the neutral extracellular medium, but is quenched upon receptor internalization and trafficking to the more acidic environments of the early and late endosomes (Yudowski *et al.*, 2006). By measuring the total fluorescence, we can track the total amount of SpH-B2AR present at the plasma membrane over time.

Cells stably expressing SpH-B2AR were transfected with mCherry-difopein or the negative control peptide. In both populations, total membrane fluorescence showed a steady decrease after cells were treated with 10 µM isoproterenol, which recovered after the agonist-containing media was replaced with media containing 40 µM alprenolol, a B2AR antagonist, causing the B2AR trafficking itinerary to become dominated by receptor recycling (Supplementary Fig. 5A-B). SpH-B2AR cells expressing the control peptide declined to a minimum of 73.05% of baseline fluorescence (95% confidence interval: 53.97-92.14%) 11 minutes after addition of isoproterenol and cells expressing difopein reaching 73.01% of baseline fluorescence (95% confidence interval: 65.04-80.99%) after the same amount of time (Supplementary Fig. 5B). After agonist removal and treatment with alprenolol, SpH-B2AR fluorescence in cells expressing the control peptide recovered to 92.91% of the initial fluorescence over 20 minutes (95% confidence interval: 85.83-99.99%), while fluorescence in cells transfected with difopein recovered to

33

92.68% of the baseline in the same time (95% confidence interval: 89.53-95.83%). There was no significant difference in the extent of either fluorescence loss after agonist treatment or recovery after washout and antagonist treatment (Supplementary Fig. 5C). Despite promoting arrestin recruitment to the receptor, 14-3-3 inhibition increases neither the rate nor extent of B2AR internalization in response to isoproterenol, nor does it impact receptor recycling back to the plasma membrane.

Discussion

Using our SILAC-based approach to identify proteins associated with activated, intracellularly-unmodified B2AR, we have generated a B2AR cross-linked interactome that captures most previously-identified B2AR interactors impacting receptor signaling and trafficking. We also identified 14-3-3 proteins as components of the B2AR cross-linked interactome that act as modifiers of adrenergic signaling via cAMP.

The dataset provided by our approach complements much of the previous work identifying B2AR interactors. Previous studies using immunoprecipitation have focused on candidate-based approaches, probing interactions with individual or small numbers of proteins (Cong *et al.*, 2001; Shenoy *et al.*, 2006; Yang *et al.*, 2010; Tian *et al.*, 2016). These characterize predicted interactions with high fidelity, but are limited in identifying new interactions. Previous unbiased screens using co-IP or protein arrays have primarily used the B2AR tail on its own (Heydorn *et al.*, 2004; He *et al.*, 2006). Such studies have generated good candidates that have been validated in our paper and others, but they may miss interactions which rely on association with multiple portions of the receptor by focusing on interactions of the tail alone. Co-IP screening using the full receptor has been attempted, but was focused on the receptor in compartments not associated with canonical signaling and agonist-stimulated trafficking (Roy *et al.*, 2013). Proximity labeling screens (Lobingier *et al.*, 2017; Paek *et al.*, 2017) have generated a rich dataset of the B2AR local interactome. It is important to distinguish that this approach requires modification of the receptor's cytoplasmic domains by inclusion of a biotinylating enzyme, which may mask interactions via steric disruption of normal protein-protein interactions (Hung *et al.*, 2016; Lobingier *et al.*, 2017). Further–while highly sensitive–the short, nonspecific labeling radius enriches proximal components, at the potential expense of components of large multiprotein complexes that are distant but still associated with the receptor. DSP cross-linking,

on the other hand, can connect successive units of large complexes, potentially increasing fidelity at capturing these types of interactions, particularly for distal components.

Comparing available datasets generated by proximity labeling to our IP-based interactome highlights the complementarity of these methods. We were able to isolate the majority of members in large complexes (Fig. 1D; Extended Data 2). These include the core retromer complex (VPS26A/B, VPS29 and VPS35) and the associated WASH complex (WASHC2/FAM21A, WASHC4/KIAA1033, and WASHC5/strumpellin), the entire CORVET complex (Beek *et al.*, 2019), and eight out of twelve members of the CCC complex (Singla *et al.*, 2019). In comparison, APEX-based proximity labeling of B2AR identified one member of WASH complex, four out of six members of CORVET, and three out of twelve CCC components (Paek *et al.*, 2017). The detection of these particular subunits by B2AR-APEX may indicate that they are oriented more closely to the receptor than other components, while cross-linked co-IP informs us that the rest of the subunits are likely present as part of a large, multi-protein complex. Therefore, it is possible that comparing results from cross-linked co-IP and proximity labeling strategies would provide structural information about the relative orientation of cargo with large sorting complexes, at least when the complex size is similar to or greater than the enzymatic labeling radius (Boesch *et al.*, 2023). While a careful structural interpretation of the interactions is outside the scope of this study, focused comparison of co-immunoprecipitiation and proximity labeling under more controlled conditions would be useful to explore the complementarity of these two approaches.

The decreased association of 14-3-3 proteins with B2AR after isoproterenol treatment was surprising and interesting. B2AR undergoes phosphorylation by multiple kinases, specifically G protein coupled receptor kinases and PKA. Based on the well-established role of 14-3-3 proteins as phosphopeptide binding partners and previous reports (Fu *et al.*, 2000; Li *et al.*,

36

2016), we expected that 14-3-3 proteins are recruited to B2AR after receptor activation. However, some prior work has suggested phosphorylation-independent 14-3-3 interactions with and phosphorylation-induced dissociation from target proteins including GPCRs (Tazawa *et al.*, 2003; Yuan *et al.*, 2019). Our demonstration of agonist-induced dissociation of 14-3-3ε from B2AR (Fig. 3A-B) indicates that the 14-3-3 protein binding identified in our crosslinked co-IP of agonist-stimulated B2AR (Fig. 1D) is a residual association, likely from B2AR remaining at or recycled to the plasma membrane. This dissociation and negative impact of 14-3-3 proteins on cAMP signaling also suggest a 14-3-3-based catecholamine signaling feedback loop. B2AR activation initiates cAMP production, which stimulates PKA. PKA can phosphorylate multiple phosphodiesterase (PDE) isoforms, promoting their activity (Degerman *et al.*, 1990; Sette *et al.*, 1994; Sette and Conti, 1996; MacKenzie *et al.*, 2002). 14-3-3 proteins then bind to phosphorylated PDEs and protect them from dephosphorylation, increasing cAMP degradation and reducing PKA activation (Pozuelo Rubio *et al.*, 2005; Palmer *et al.*, 2007; Vandeput *et al.*, 2013). Considering the emerging model that the global cAMP response is an integrated response of multiple discrete cAMP signaling nanodomains generated by high concentrations of active PDE in the cytoplasm, 14-3-3 proteins bound to B2AR and released upon receptor activation could contribute to sharper cAMP gradients by locally modifying PDE activity (Anton *et al.*, 2022).

The selective effect of 14-3-3 on cAMP, but not on ERK, downstream of B2AR further demonstrates the potential for pathway-dependent regulation. The exact signaling pathways by which B2AR activation promotes ERK phosphorylation are still being debated, and could depend on the cell types and culture conditions used. ERK activation downstream of B2AR has been variously attributed to arrestin-mediated activation of components of the MAP Kinase pathway and to Gi-mediated activation (Shenoy *et al.*, 2006; O'Hayre *et al.*, 2017; Luttrell *et al.*, 2018; Kahsai *et al.*, 2023). However, recent evidence shows that at least a portion of B2AR-

37

induced ERK signaling requires activation of $G\alpha_s$ at endosomes following agonist-induced internalization, suggesting a pathway involving $G\alpha_s$ association with Raf1 (Kwon *et al.*, 2022). It is possible that ERK activation could be via direct receptor interactions with downstream activators of the pathway. It is also possible that the amplification steps make it difficult to detect smaller changes when endogenous elements are saturating in this system. Taken together our study indicates B2AR-stimulated that ERK activation is less sensitive than cAMP production to 14-3-3 proteins.

Overall, our results support a model where 14-3-3 proteins regulate adrenergic signaling by establishing a sequestered population of receptors at the cell surface (Fig. 8). The biggest change we see upon 14-3-3 inhibition is an increase in total cAMP accumulation, with minimal shift in the concentration-response curve. Further, we also see an increase in total miniGs and arrestin recruitment, with similar shift in the concentration-response. These imply that 14-3-3 proteins act by reducing the total amount of B2AR available to interact with effectors, establishing an inactive reserve: a population of receptors unavailable for signaling upon acute agonist stimulation. Our results at this stage cannot distinguish whether this insensitivity is because 14-3-3 proteins keep receptors in a conformation incapable of binding ligands, or because the receptor cannot interact with effectors even when bound to ligand. Because the canonical role for 14-3-3 proteins is to act as a scaffold to occlude binding effectors, it is likely that 14-3-3 acts by occluding G protein binding via steric hindrance, irrespective of ligand binding. When the non-reserve B2AR is internalized upon activation, the equilibrium at the plasma membrane shifts toward 14-3-3 dissociation, freeing up B2AR for binding to effectors once activated. Such a mechanism would prevent overstimulation in response to acute increases in agonist and ensure that prolonged stimulation causes a persistent signal, as opposed to an acute spike followed by a prolonged period of cellular desensitization. A 14-3-3-dependent inactive pool could therefore dampen the amplitude and lengthen the temporal

38

response of B2AR activation.

14-3-3 proteins are widely distributed, and could be part of a general mechanism for controlling receptor availability for signaling. Because 14-3-3 proteins typically act as dimers, they could form functionally-distinct complexes specific for different receptors, a possibility supported by reports of a particular role for 14-3-3γ in extended kappa opioid receptor inhibition (Wedemeyer *et al.*, 2022). 14-3-3ε was the most abundant isoform in our dataset, and is known almost exclusively to form heterodimers with other isoforms (Chaudhri *et al.*, 2003; Yang *et al.*, 2006). It is possible that 14-3-3ε acts through association with ζ/δ and θ–the other two most abundant isoforms in our dataset. This is consistent with our data that overexpressing ε alone does not change B2AR signaling, possibly due to the high endogenous expression of 14-3-3 proteins saturating the receptors available for sequestration (Supplementary Fig. 4). Together, our results reveal a mechanism where 14-3-3 or analogous proteins keep GPCRs in an inactive pool, controlling the amplitude and temporal characteristics of receptor activation at population levels, without specifically modifying activation kinetics of individual receptors. As receptor sequestration would be expected to regulate adrenergic signaling in important physiological systems, our findings offer a new point for modulating B2AR response to stimulation. By demonstrating that 14-3-3 proteins act as important regulators of B2AR signaling, we also gain confidence that the additional novel or understudied B2AR-interacting proteins identified by our proteomic screen represent legitimate partners with meaningful roles that have yet to be revealed.

Acknowledgements

Data Availability Statement

The authors declare that all the data supporting the findings of this study are available within the

paper and its Supplemental Data.

Author Contributions

IC, RV, AG, VF, and MP participated in research design. IC, RV, and AG conducted experiments. IC, MP, and VF performed data analysis. IC, MP, RV, AG, and VF wrote or contributed to the writing of the manuscript.

References

Aghazadeh Y, and Papadopoulos V (2016) The role of the 14-3-3 protein family in health, disease, and drug development. *Drug Discov Today* **21**:278–287.

Anton SE, Kayser C, Maiellaro I, Nemec K, Möller J, Koschinski A, Zaccolo M, Annibale P, Falcke M, Lohse MJ, and Bock A (2022) Receptor-associated independent cAMP nanodomains mediate spatiotemporal specificity of GPCR signaling. *Cell*, doi: 10.1016/j.cell.2022.02.011.

Ashburner M, Ball CA, Blake JA, Botstein D, Butler H, Cherry JM, Davis AP, Dolinski K, Dwight SS, Eppig JT, Harris MA, Hill DP, Issel-Tarver L, Kasarskis A, Lewis S, Matese JC, Richardson JE, Ringwald M, Rubin GM, and Sherlock G (2000) Gene Ontology: tool for the unification of biology. *Nat Genet* **25**:25–29, Nature Publishing Group.

Bader GD, and Hogue CW (2003) An automated method for finding molecular complexes in large protein interaction networks. *BMC Bioinformatics* **4**:2.

Bauman AL, Soughayer J, Nguyen BT, Willoughby D, Carnegie GK, Wong W, Hoshi N, Langeberg LK, Cooper DMF, Dessauer CW, and Scott JD (2006) Dynamic Regulation of cAMP Synthesis through Anchored PKA-Adenylyl Cyclase V/VI Complexes. *Mol Cell* **23**:925–931.

Beek J van der, Jonker C, Welle R van der, Liv N, and Klumperman J (2019) CORVET, CHEVI and HOPS – multisubunit tethers of the endo-lysosomal system in health and disease. *J Cell Sci* **132**, The Company of Biologists Ltd.

Besson B, Eun H, Kim S, Windisch MP, Bourhy H, and Grailhe R (2022) Optimization of BRET saturation assays for robust and sensitive cytosolic protein–protein interaction studies. *Sci Rep* **12**:9987, Nature Publishing Group.

Binkowski BF, Butler BL, Stecha PF, Eggers CT, Otto P, Zimmerman K, Vidugiris G, Wood MG, Encell LP, Fan F, and Wood KV (2011) A Luminescent Biosensor with Increased Dynamic Range for Intracellular cAMP. *ACS Chem Biol* **6**:1193–1197, American Chemical Society.

Boesch DJ, Singla A, Han Y, Kramer DA, Liu Q, Suzuki K, Juneja P, Zhao X, Long X, Medlyn MJ, Billadeau DD, Chen Z, Chen B, and Burstein E (2023) Structural organization of the retriever–CCC endosomal recycling complex. *Nat Struct Mol Biol* 1–15, Nature Publishing Group.

Buchwald P (2019) A Receptor Model With Binding Affinity, Activation Efficacy, and Signal Amplification Parameters for Complex Fractional Response Versus Occupancy Data. *Front Pharmacol* **10**, Frontiers.

Bylund DB (2006) Adrenergic Receptors, in *The Adrenergic Receptors: In the 21st Century* (Perez DM ed) pp 3–21, Humana Press, Totowa, NJ.

Cao TT, Deacon HW, Reczek D, Bretscher A, and von Zastrow M (1999) A kinase-regulated PDZ-domain interaction controls endocytic sorting of the beta2-adrenergic receptor. *Nature* **401**:286–290.

Cell line - SFN - The Human Protein Atlas (n.d.). https://www.proteinatlas.org/ENSG00000175793-SFN/cell+line.

Cell line - YWHAE - The Human Protein Atlas (n.d.). https://www.proteinatlas.org/ENSG00000108953-YWHAE/cell+line.

Chaudhri M, Scarabel M, and Aitken A (2003) Mammalian and yeast 14-3-3 isoforms form distinct patterns of dimers in vivo. *Biochem Biophys Res Commun* **300**:679–685.

Cho NH, Cheveralls KC, Brunner A-D, Kim K, Michaelis AC, Raghavan P, Kobayashi H, Savy L, Li JY, Canaj H, Kim JYS, Stewart EM, Gnann C, McCarthy F, Cabrera JP, Brunetti RM, Chhun BB, Dingle G, Hein MY, Huang B, Mehta SB, Weissman JS, Gómez-Sjöberg R, Itzhak DN, Royer LA, Mann M, and Leonetti MD (2022) OpenCell: Endogenous tagging for the cartography of human cellular organization. *Science* **375**:eabi6983, American Association for the Advancement of Science.

Christoforidis S, McBride HM, Burgoyne RD, and Zerial M (1999) The Rab5 effector EEA1 is a core component of endosome docking. *Nature* **397**:621–625, Nature Publishing Group.

Cianfrocco MA, Wong-Barnum M, Youn C, Wagner R, and Leschziner A (2017) COSMIC2: A Science Gateway for Cryo-Electron Microscopy Structure Determination, in *Proceedings of the Practice and Experience in Advanced Research Computing 2017 on Sustainability, Success and Impact* pp 1–5, Association for Computing Machinery, New York, NY, USA.

Cong M, Perry SJ, Hu LA, Hanson PI, Claing A, and Lefkowitz RJ (2001) Binding of the beta2 adrenergic receptor to N-ethylmaleimide-sensitive factor regulates receptor recycling. *J Biol Chem* **276**:45145–45152.

Degerman E, Smith CJ, Tornqvist H, Vasta V, Belfrage P, and Manganiello VC (1990) Evidence that insulin and isoprenaline activate the cGMP-inhibited low-Km cAMP phosphodiesterase in rat fat cells by phosphorylation. *Proc Natl Acad Sci* **87**:533–537, Proceedings of the National Academy of Sciences.

Dixon AS, Schwinn MK, Hall MP, Zimmerman K, Otto P, Lubben TH, Butler BL, Binkowski BF, Machleidt T, Kirkland TA, Wood MG, Eggers CT, Encell LP, and Wood KV (2016) NanoLuc Complementation Reporter Optimized for Accurate Measurement of Protein Interactions in Cells. *ACS Chem Biol* **11**:400–408, American Chemical Society.

Drury DEJ, Chong LK, Ghahramani P, and Peachell PT (1998) Influence of receptor reserve on β-adrenoceptor-mediated responses in human lung mast cells. *Br J Pharmacol* **124**:711–718.

Evans R, O'Neill M, Pritzel A, Antropova N, Senior A, Green T, Žídek A, Bates R, Blackwell S, Yim J, Ronneberger O, Bodenstein S, Zielinski M, Bridgland A, Potapenko A, Cowie A, Tunyasuvunakool K, Jain R, Clancy E, Kohli P, Jumper J, and Hassabis D (2022) Protein complex prediction with AlphaFold-Multimer, bioRxiv.

Fraser IDC, Cong M, Kim J, Rollins EN, Daaka Y, Lefkowitz RJ, and Scott JD (2000) Assembly of an A kinase-anchoring protein–β2-adrenergic receptor complex facilitates receptor phosphorylation and signaling. *Curr Biol* **10**:409–412.

Fu H, Subramanian RR, and Masters SC (2000) 14-3-3 Proteins: Structure, Function, and Regulation. *Annu Rev Pharmacol Toxicol* **40**:617–647.

Giembycz MA (2009) An estimation of β2-adrenoceptor reserve on human bronchial smooth muscle for some sympathomimetic bronchodilators. *Br J Pharmacol* **158**:287–299.

Gokhale A, Larimore J, Werner E, So L, Moreno-De-Luca A, Lese-Martin C, Lupashin VV, Smith Y, and Faundez V (2012) Quantitative Proteomic and Genetic Analyses of the Schizophrenia Susceptibility Factor Dysbindin Identify Novel Roles of the Biogenesis of Lysosome-Related Organelles Complex 1. *J Neurosci* **32**:3697–3711.

Gokhale A, Perez-Cornejo P, Duran C, Hartzell HC, and Faundez V (2012) A comprehensive strategy to identify stoichiometric membrane protein interactomes. *Cell Logist* **2**:189–196.

Gokhale A, Ryder PV, Zlatic SA, and Faundez V (2016) Identification of the Interactome of a Palmitoylated Membrane Protein, Phosphatidylinositol 4-Kinase Type II Alpha. *Methods Mol Biol Clifton NJ* **1376**:35–42.

Gomez TS, and Billadeau DD (2009) A FAM21-Containing WASH Complex Regulates Retromer-Dependent Sorting. *Dev Cell* **17**:699–711.

Grant MP, Stepanchick A, Cavanaugh A, and Breitwieser GE (2011) Agonist-Driven Maturation and Plasma Membrane Insertion of Calcium-Sensing Receptors Dynamically Control Signal Amplitude. *Sci Signal* **4**:ra78–ra78, American Association for the Advancement of Science.

Hall RA, Premont RT, Chow C-W, Blitzer JT, Pitcher JA, Claing A, Stoffel RH, Barak LS, Shenolikar S, Weinman EJ, Grinstein S, and Lefkowitz RJ (1998) The β2-adrenergic receptor interacts with the Na+/H+-exchanger regulatory factor to control Na+/H+ exchange. *Nature* **392**:626–630.

He J, Bellini M, Inuzuka H, Xu J, Xiong Y, Yang X, Castleberry AM, and Hall RA (2006) Proteomic Analysis of β1-Adrenergic Receptor Interactions with PDZ Scaffold Proteins*. *J Biol Chem* **281**:2820–2827.

Heng J, Hu Y, Pérez-Hernández G, Inoue A, Zhao J, Ma X, Sun X, Kawakami K, Ikuta T, Ding J, Yang Y, Zhang L, Peng S, Niu X, Li H, Guixà-González R, Jin C, Hildebrand PW, Chen C, and Kobilka BK (2023) Function and dynamics of the intrinsically disordered carboxyl terminus of β2 adrenergic receptor. *Nat Commun* **14**:2005, Nature Publishing Group.

Heydorn A, Søndergaard BP, Ersbøll B, Holst B, Nielsen FC, Haft CR, Whistler J, and Schwartz TW (2004) A Library of 7TM Receptor C-terminal Tails: INTERACTIONS WITH THE PROPOSED POST-ENDOCYTIC SORTING PROTEINS ERM-BINDING PHOSPHOPROTEIN 50 (EBP50), N-ETHYLMALEIMIDE-SENSITIVE FACTOR (NSF), SORTING NEXIN 1 (SNX1), AND G PROTEIN-COUPLED RECEPTOR-ASSOCIATED SORTING PROTEIN (GASP)*. *J Biol Chem* **279**:54291–54303.

Hung V, Udeshi ND, Lam SS, Loh KH, Cox KJ, Pedram K, Carr SA, and Ting AY (2016) Spatially resolved proteomic mapping in living cells with the engineered peroxidase APEX2. *Nat Protoc* **11**:456–475.

Irannejad R, Tomshine JC, Tomshine JR, Chevalier M, Mahoney JP, Steyaert J, Rasmussen SGF, Sunahara RK, El-Samad H, Huang B, and von Zastrow M (2013) Conformational biosensors reveal GPCR signalling from endosomes. *Nature* **495**:534–538.

Johnson M (1998) The β -Adrenoceptor. *Am J Respir Crit Care Med* **158**:S146–S153, American Thoracic Society - AJRCCM.

Jumper J, Evans R, Pritzel A, Green T, Figurnov M, Ronneberger O, Tunyasuvunakool K, Bates R, Žídek A, Potapenko A, Bridgland A, Meyer C, Kohl SAA, Ballard AJ, Cowie A, Romera-Paredes B, Nikolov S, Jain R, Adler J, Back T, Petersen S, Reiman D, Clancy E, Zielinski M, Steinegger M, Pacholska M, Berghammer T, Bodenstein S, Silver D, Vinyals O, Senior AW, Kavukcuoglu K, Kohli P, and Hassabis D (2021) Highly accurate protein structure prediction with AlphaFold. *Nature* **596**:583–589, Nature Publishing Group.

Kahsai AW, Shah KS, Shim PJ, Lee MA, Shreiber BN, Schwalb AM, Zhang X, Kwon HY, Huang L-Y, Soderblom EJ, Ahn S, and Lefkowitz RJ (2023) Signal transduction at GPCRs: Allosteric activation of the ERK MAPK by β-arrestin. *Proc Natl Acad Sci* **120**:e2303794120, Proceedings of the National Academy of Sciences.

Karoor V, Wang L, Wang H, and Malbon CC (1998) Insulin Stimulates Sequestration of β-Adrenergic Receptors and Enhanced Association of β-Adrenergic Receptors with Grb2 via Tyrosine 350*. *J Biol Chem* **273**:33035–33041.

Kwon Y, Mehta S, Clark M, Walters G, Zhong Y, Lee HN, Sunahara RK, and Zhang J (2022) Non-canonical β-adrenergic activation of ERK at endosomes. *Nature* 1–7, Nature Publishing Group.

Lauffer BEL, Melero C, Temkin P, Lei C, Hong W, Kortemme T, and von Zastrow M (2010) SNX27 mediates PDZ-directed sorting from endosomes to the plasma membrane. *J Cell Biol* **190**:565–574.

Lefkowitz RJ (2007) Seven transmembrane receptors—A brief personal retrospective. *Biochim Biophys Acta BBA - Biomembr* **1768**:748–755.

Li F-Q, Mofunanya A, Harris K, and Takemaru K-I (2008) Chibby cooperates with 14-3-3 to regulate beta-catenin subcellular distribution and signaling activity. *J Cell Biol* **181**:1141–1154.

Li H, Eishingdrelo A, Kongsamut S, and Eishingdrelo H (2016) G-protein-coupled receptors mediate 14-3-3 signal transduction. *Signal Transduct Target Ther* **1**:1–8, Nature Publishing Group.

Liao Y, Wang J, Jaehnig EJ, Shi Z, and Zhang B (2019) WebGestalt 2019: gene set analysis toolkit with revamped UIs and APIs. *Nucleic Acids Res* **47**:W199–W205.

Lobingier BT, Hüttenhain R, Eichel K, Miller KB, Ting AY, von Zastrow M, and Krogan NJ (2017) An Approach to Spatiotemporally Resolve Protein Interaction Networks in Living Cells. *Cell* **169**:350-360.e12.

Luttrell LM, Wang J, Plouffe B, Smith JS, Yamani L, Kaur S, Jean-Charles P-Y, Gauthier C, Lee M-H, Pani B, Kim J, Ahn S, Rajagopal S, Reiter E, Bouvier M, Shenoy SK, Laporte SA, Rockman HA, and Lefkowitz RJ (2018) Manifold roles of β-arrestins in GPCR signaling elucidated with siRNA and CRISPR/Cas9. *Sci Signal* **11**:eaat7650.

MacKenzie SJ, Baillie GS, McPhee I, MacKenzie C, Seamons R, McSorley T, Millen J, Beard MB, van Heeke G, and Houslay MD (2002) Long PDE4 cAMP specific phosphodiesterases are activated by protein kinase A-mediated phosphorylation of a single serine residue in Upstream Conserved Region 1 (UCR1). *Br J Pharmacol* **136**:421–433.

Maïssa N, Covarelli V, Janel S, Durel B, Simpson N, Bernard SC, Pardo-Lopez L, Bouzinba-Ségard H, Faure C, Scott MGH, Coureuil M, Morand PC, Lafont F, Nassif X, Marullo S, and Bourdoulous S (2017) Strength of Neisseria meningitidis binding to endothelial cells requires highly-ordered CD147/β2-adrenoceptor clusters assembled by alpha-actinin-4. *Nat Commun* **8**:15764.

Mariani V, Biasini M, Barbato A, and Schwede T (2013) lDDT: a local superposition-free score for comparing protein structures and models using distance difference tests. *Bioinformatics* **29**:2722–2728.

Masters SC, and Fu H (2001) 14-3-3 Proteins Mediate an Essential Anti-apoptotic Signal *. *J Biol Chem* **276**:45193–45200, Elsevier.

Moore RH, Millman EE, Alpizar-Foster E, Dai W, and Knoll BJ (2004) Rab11 regulates the recycling and lysosome targeting of β2-adrenergic receptors. *J Cell Sci* **117**:3107–3117.

O'Hayre M, Eichel K, Avino S, Zhao X, Steffen DJ, Feng X, Kawakami K, Aoki J, Messer K, Sunahara R, Inoue A, von Zastrow M, and Gutkind JS (2017) Genetic evidence that β-arrestins are dispensable for the initiation of β2-adrenergic receptor signaling to ERK. *Sci Signal* **10**.

Oughtred R, Rust J, Chang C, Breitkreutz B, Stark C, Willems A, Boucher L, Leung G, Kolas N, Zhang F, Dolma S, Coulombe-Huntington J, Chatr-aryamontri A, Dolinski K, and Tyers M (2021) The BioGRID database: A comprehensive biomedical resource of curated protein, genetic, and chemical interactions. *Protein Sci Publ Protein Soc* **30**:187–200.

Paek J, Kalocsay M, Staus DP, Wingler L, Pascolutti R, Paulo JA, Gygi SP, and Kruse AC (2017) Multidimensional Tracking of GPCR Signaling via Peroxidase-Catalyzed Proximity Labeling. *Cell* **169**:338-349.e11.

Palmer D, Jimmo SL, Raymond DR, Wilson LS, Carter RL, and Maurice DH (2007) Protein Kinase A Phosphorylation of Human Phosphodiesterase 3B Promotes 14-3-3 Protein Binding and Inhibits Phosphatase-catalyzed Inactivation *. *J Biol Chem* **282**:9411–9419, Elsevier.

Pennington KL, Chan TY, Torres MP, and Andersen JL (2018) The dynamic and stress-adaptive signaling hub of 14-3-3: emerging mechanisms of regulation and context-dependent protein–protein interactions. *Oncogene* **37**:5587–5604, Nature Publishing Group.

Perez-Cornejo P, Gokhale A, Duran C, Cui Y, Xiao Q, Hartzell HC, and Faundez V (2012) Anoctamin 1 (Tmem16A) Ca2+-activated chloride channel stoichiometrically interacts with an ezrin-radixin-moesin network. *Proc Natl Acad Sci U S A* **109**:10376–10381.

Perry SJ, Baillie GS, Kohout TA, McPhee I, Magiera MM, Ang KL, Miller WE, McLean AJ, Conti M, Houslay MD, and Lefkowitz RJ (2002) Targeting of Cyclic AMP Degradation to β2-Adrenergic Receptors by β-Arrestins. *Science* **298**:834–836, American Association for the Advancement of Science.

Pettersen EF, Goddard TD, Huang CC, Meng EC, Couch GS, Croll TI, Morris JH, and Ferrin TE (2021) UCSF ChimeraX: Structure visualization for researchers, educators, and developers. *Protein Sci Publ Protein Soc* **30**:70–82.

Pierce KL, Premont RT, and Lefkowitz RJ (2002) Seven-transmembrane receptors. *Nat Rev Mol Cell Biol* **3**:639–650.

Pons M, Izquierdo I, Andreu-Carbó M, Garrido G, Planagumà J, Muriel O, del Pozo MA, Geli MI, and Aragay AM (2017) Phosphorylation of filamin A regulates chemokine receptor CCR2 recycling. *J Cell Sci* **130**:490–501.

Pozuelo Rubio M, Campbell DG, Morrice NA, and Mackintosh C (2005) Phosphodiesterase 3A binds to 14-3-3 proteins in response to PMA-induced phosphorylation of Ser428. *Biochem J* **392**:163–172.

Puthenveedu MA, Lauffer B, Temkin P, Vistein R, Carlton P, Thorn K, Taunton J, Weiner OD, Parton RG, and von Zastrow M (2010) Sequence-Dependent Sorting of Recycling Proteins by Actin-Stabilized Endosomal Microdomains. *Cell* **143**:761–773.

Roy SJ, Glazkova I, Fréchette L, Iorio-Morin C, Binda C, Pétrin D, Trieu P, Robitaille M, Angers S, Hébert TE, and Parent J-L (2013) Novel, Gel-free Proteomics Approach Identifies RNF5 and JAMP as Modulators of GPCR Stability. *Mol Endocrinol* **27**:1245–1266.

Ryder PV, Vistein R, Gokhale A, Seaman MN, Puthenveedu MA, and Faundez V (2013a) The WASH complex, an endosomal Arp2/3 activator, interacts with the Hermansky-Pudlak syndrome complex BLOC-1 and its cargo phosphatidylinositol-4-kinase type IIα. *Mol Biol Cell* **24**:2269–2284.

Ryder PV, Vistein R, Gokhale A, Seaman MN, Puthenveedu MA, and Faundez V (2013b) The WASH complex, an endosomal Arp2/3 activator, interacts with the Hermansky–Pudlak syndrome complex BLOC-1 and its cargo phosphatidylinositol-4-kinase type IIα. *Mol Biol Cell* **24**:2269–2284.

Sette C, and Conti M (1996) Phosphorylation and Activation of a cAMP-specific Phosphodiesterase by the cAMP-dependent Protein Kinase: INVOLVEMENT OF SERINE 54 IN THE ENZYME ACTIVATION*. *J Biol Chem* **271**:16526–16534.

Sette C, Vicini E, and Conti M (1994) The ratPDE3/IVd phosphodiesterase gene codes for multiple proteins differentially activated by cAMP-dependent protein kinase. *J Biol Chem* **269**:18271–18274.

Shenoy SK, Drake MT, Nelson CD, Houtz DA, Xiao K, Madabushi S, Reiter E, Premont RT, Lichtarge O, and Lefkowitz RJ (2006) beta-arrestin-dependent, G protein-independent ERK1/2 activation by the beta2 adrenergic receptor. *J Biol Chem* **281**:1261–1273.

Singla A, Fedoseienko A, Giridharan SSP, Overlee BL, Lopez A, Jia D, Song J, Huff-Hardy K, Weisman L, Burstein E, and Billadeau DD (2019) Endosomal PI(3)P regulation by the COMMD/CCDC22/CCDC93 (CCC) complex controls membrane protein recycling. *Nat Commun* **10**:4271, Nature Publishing Group.

Sriram K, and Insel PA (2018) G Protein-Coupled Receptors as Targets for Approved Drugs: How Many Targets and How Many Drugs? *Mol Pharmacol* **93**:251–258.

Szklarczyk D, Gable AL, Lyon D, Junge A, Wyder S, Huerta-Cepas J, Simonovic M, Doncheva NT, Morris JH, Bork P, Jensen LJ, and Mering C von (2019) STRING v11: protein–protein association networks with increased coverage, supporting functional discovery in genome-wide experimental datasets. *Nucleic Acids Res* **47**:D607–D613.

Tazawa H, Takahashi S, and Zilliacus J (2003) Interaction of the parathyroid hormone receptor with the 14-3-3 protein. *Biochim Biophys Acta BBA - Gen Subj* **1620**:32–38.

Terasaki WL, Linden J, and Brooker G (1979) Quantitative relationship between β-adrenergic receptor number and physiologic responses as studied with a long-lasting β-adrenergic antagonist. *Proc Natl Acad Sci U S A* **76**:6401–6405.

The Gene Ontology Consortium, Aleksander SA, Balhoff J, Carbon S, Cherry JM, Drabkin HJ, Ebert D, Feuermann M, Gaudet P, Harris NL, Hill DP, Lee R, Mi H, Moxon S, Mungall CJ, Muruganugan A, Mushayahama T, Sternberg PW, Thomas PD, Van Auken K, Ramsey J, Siegele DA, Chisholm RL, Fey P, Aspromonte MC, Nugnes MV, Quaglia F, Tosatto S, Giglio M, Nadendla S, Antonazzo G, Attrill H, dos Santos G, Marygold S, Strelets V, Tabone CJ, Thurmond J, Zhou P, Ahmed SH, Asanitthong P, Luna Buitrago D, Erdol MN, Gage MC, Ali Kadhum M, Li KYC, Long M, Michalak A, Pesala A, Pritazahra A, Saverimuttu SCC, Su R, Thurlow KE, Lovering RC, Logie C, Oliferenko S, Blake J, Christie K, Corbani L, Dolan ME, Drabkin HJ, Hill DP, Ni L, Sitnikov D, Smith C, Cuzick A, Seager J, Cooper L, Elser J, Jaiswal P, Gupta P, Jaiswal P, Naithani S, Lera-Ramirez M, Rutherford K, Wood V, De Pons JL, Dwinell MR, Hayman GT, Kaldunski ML, Kwitek AE, Laulederkind SJF, Tutaj MA, Vedi M, Wang S-J, D'Eustachio P, Aimo L, Axelsen K, Bridge A, Hyka-Nouspikel N, Morgat A, Aleksander SA, Cherry JM, Engel SR, Karra K, Miyasato SR, Nash RS, Skrzypek MS, Weng S, et al. (2023) The Gene Ontology knowledgebase in 2023. *Genetics* **224**:iyad031.

Thompson WC, and Goldspink PH (2022) 14–3-3 protein regulation of excitation–contraction coupling. *Pflugers Arch* **474**:267–279.

Tian X, Irannejad R, Bowman SL, Du Y, Puthenveedu MA, von Zastrow M, and Benovic JL (2016) The α-Arrestin ARRDC3 Regulates the Endosomal Residence Time and Intracellular Signaling of the β_2-Adrenergic Receptor. *J Biol Chem* **291**:14510–14525.

Tsvetanova NG, and von Zastrow M (2014) Spatial encoding of cyclic AMP signaling specificity by GPCR endocytosis. *Nat Chem Biol* **10**:1061–1065.

Tunyasuvunakool K, Adler J, Wu Z, Green T, Zielinski M, Žídek A, Bridgland A, Cowie A, Meyer C, Laydon A, Velankar S, Kleywegt GJ, Bateman A, Evans R, Pritzel A, Figurnov M, Ronneberger O, Bates R, Kohl SAA, Potapenko A, Ballard AJ, Romera-Paredes B, Nikolov S, Jain R, Clancy E, Reiman D, Petersen S, Senior AW, Kavukcuoglu K, Birney E, Kohli P, Jumper J, and Hassabis D (2021) Highly accurate protein structure prediction for the human proteome. *Nature* **596**:590–596, Nature Publishing Group.

Tutor AS, Delpón E, Caballero R, Gómez R, Núñez L, Vaquero M, Tamargo J, Mayor F, and Penela P (2006) Association of 14-3-3 proteins to beta1-adrenergic receptors modulates Kv11.1 K+ channel activity in recombinant systems. *Mol Biol Cell* **17**:4666–4674.

Uhlén M, Fagerberg L, Hallström BM, Lindskog C, Oksvold P, Mardinoglu A, Sivertsson Å, Kampf C, Sjöstedt E, Asplund A, Olsson I, Edlund K, Lundberg E, Navani S, Szigyarto CA-K, Odeberg J, Djureinovic D, Takanen JO, Hober S, Alm T, Edqvist P-H, Berling H, Tegel H, Mulder J, Rockberg J, Nilsson P, Schwenk JM, Hamsten M, von Feilitzen K, Forsberg M, Persson L, Johansson F, Zwahlen M, von Heijne G, Nielsen J, and Pontén F (2015) Tissue-based map of the human proteome. *Science* **347**:1260419, American Association for the Advancement of Science.

Ullrich O, Reinsch S, Urbé S, Zerial M, and Parton RG (1996) Rab11 regulates recycling through the pericentriolar recycling endosome. *J Cell Biol* **135**:913–924.

Vandeput F, Szabo-Fresnais N, Ahmad F, Kho C, Lee A, Krall J, Dunlop A, Hazel MW, Wohlschlegel JA, Hajjar RJ, Houslay MD, Manganiello VC, and Movsesian MA (2013) Selective regulation of cyclic nucleotide phosphodiesterase PDE3A isoforms. *Proc Natl Acad Sci* **110**:19778–19783, Proceedings of the National Academy of Sciences.

Varandas KC, Irannejad R, and von Zastrow M (2016) Retromer Endosome Exit Domains Serve Multiple Trafficking Destinations and Regulate Local G Protein Activation by GPCRs. *Curr Biol CB* **26**:3129–3142.

Venter JC (1979) High Efficiency Coupling Between Beta-adrenergic Receptors and Cardiac Contractility: Direct Evidence for "Spare" Beta-adrenergic Receptors. *Mol Pharmacol* **16**:429–440, American Society for Pharmacology and Experimental Therapeutics.

Vistein R, and Puthenveedu MA (2014) Src regulates sequence-dependent beta-2 adrenergic receptor recycling via cortactin phosphorylation. *Traffic Cph Den* **15**:1195–1205.

Wedemeyer MJ, Jennings EM, Smith HR, Chavera TS, Jamshidi RJ, Berg KA, and Clarke WP (2022) 14-3-3γ mediates the long-term inhibition of peripheral kappa opioid receptor antinociceptive signaling by norbinaltorphimine. *Neuropharmacology* **220**:109251.

Wolfe BL, and Trejo J (2007) Clathrin-Dependent Mechanisms of G Protein-coupled Receptor Endocytosis. *Traffic* **8**:462–470.

Yang Q, Loureiro ZY, Desai A, DeSouza T, Li K, Wang H, Nicoloro SM, Solivan-Rivera J, and Corvera S (2023) Regulation of lipolysis by 14-3-3 proteins on human adipocyte lipid droplets. *PNAS Nexus* **2**:pgad420.

Yang X, Lee WH, Sobott F, Papagrigoriou E, Robinson CV, Grossmann JG, Sundström M, Doyle DA, and Elkins JM (2006) Structural basis for protein–protein interactions in the 14-3-3 protein family. *Proc Natl Acad Sci U S A* **103**:17237–17242.

Yang X, Zheng J, Xiong Y, Shen H, Sun L, Huang Y, Sun C, Li Y, and He J (2010) Beta-2 adrenergic receptor mediated ERK activation is regulated by interaction with MAGI-3. *FEBS Lett* **584**:2207–2212.

Yuan L, Barbash S, Kongsamut S, Eishingdrelo A, Sakmar TP, and Eishingdrelo H (2019) 14-3-3 signal adaptor and scaffold proteins mediate GPCR trafficking. *Sci Rep* **9**.

Yudowski GA, Puthenveedu MA, and von Zastrow M (2006) Distinct modes of regulated receptor insertion to the somatodendritic plasma membrane. *Nat Neurosci* **9**:622–627, Nature Publishing Group.

Zeigerer A, Gilleron J, Bogorad RL, Marsico G, Nonaka H, Seifert S, Epstein-Barash H, Kuchimanchi S, Peng CG, Ruda VM, Conte-Zerial PD, Hengstler JG, Kalaidzidis Y, Koteliansky V, and Zerial M (2012) Rab5 is necessary for the biogenesis of the endolysosomal system in vivo. *Nature* **485**:465–470, Nature Publishing Group.

Footnotes

No author has an actual or perceived conflict of interest with the contents of this article.

Legends for Figures

Figure 1

SILAC co-immunoprecipitation identifies 14-3-3 proteins as B2AR interacting proteins. A) FLAG-B2AR labeled with anti-FLAG-AlexaFluor 647 is present at the plasma membrane in HEK293 cells and internalizes in response to treatment with 10 µM isoproterenol for 10 minutes, as visualized using confocal microscopy. B) Silver stain of proteins from the whole cell lysate/input (left) and FLAG mAb co-immunoprecipitation elute (right) with HEK293 cells stably expressing FLAG-B2AR. B) Schematic showing the procedure used for SILAC co-immunoprecipitation and preliminary processing of the results. D) Cross-linked co-immunoprecipitation with anti-FLAG antibodies in HEK293 cells stably expressing FLAG-B2AR identify many known B2AR-interacting proteins enriched over samples pulled down in the presence of an excess of antigenic FLAG peptide. Multiple 14-3-3 isoforms are identified as preferentially associating with FLAG-B2AR over the negative control.

Figure 2

Co-IP identifies B2AR-interactors involved in cargo sorting and trafficking. A) Gene ontology analysis using WebGestalt identifies overrepresentation of identified B2AR-interacting proteins in biological pathways related to protein and membrane trafficking. B) The protein-protein interaction algorithm Molecular Complex Detection (MCODE) was used to identify proteins clustered based on previously-established interactions compiled by STRING and BioGRID. Multiple complexes involved in cargo sorting at endosomes were identified.

Figure 3

14-3-3 protein interaction with B2AR is decreased by receptor stimulation. A) Co-immunoprecipitation of HA-14-3-3ε with FLAG-B2AR in HEK293 cells expressing stably

expressing FLAG-B2AR in the presence of 10 μM iso or H_2O vehicle and in a parental control HEK293 cell line. B) Quantification of Fig. 3A. Data are shown as the ratio of HA-14-3-3ε in the sample elute to input, displayed as a percent of the amount in the FLAG-B2AR cells treated with H_2O vehicle (mean ± 95% confidence interval, n=3, Paired, one-way ANOVA with Dunnet's correction for multiple comparisons; FLAG-B2AR vehicle vs. iso: p=0.0479; FLAG-B2AR vehicle vs. non-expressing control: p=0.0016). C) Schematic of B2AR-APEX proximity labeling. APEX irreversibly biotinylates proteins adjacent to the B2AR-APEX construct in living cells. D) Biotinylation of transfected HA-14-3-3ε in HEK293 cells stably expressing FLAG-B2AR-APEX treated with 10 μM isoproterenol or vehicle for 10 minutes followed by 1 mM H_2O_2 or vehicle for 1 minute. E) Schematic of the NanoBit luciferase complementation assay. Association of B2AR-LgBit and SmBit-14-3-3ε leads to an increase in luminescence. F) Baseline luminescence in HEK293 cells transfected with 5 ng B2AR-LgBit and increasing concentrations of SmBit-14-3-3ε, shown as a fold change over cells transfected with 1 ng SmBit-14-3-3ε (n=3). G) Timecourse of corrected luminescence in cells expressing B2AR-LgBit and SmBit-14-3-3ε treated with 10 μM isoproterenol (Iso; blue) or a media vehicle (grey). Traces represent mean values of 6 independent experiments (±standard deviation), shown as a percentage of the average value before treatment. H) AlphaFold Multimer top structural prediction of B2AR (blue) bound to 14-3-3ε (orange) and 14-3-3ζ/δ (gold). The first twenty amino acids of the B2AR N-terminus have been removed for spatial concision, but were included during structure prediction. I) Predicted local distance difference test (pLDDT) values for all residues of the top predicted structure shown in A for B2AR, 14-3-3ε, and 14-3-3ζ/δ. Values below 50 (dotted line) are very low confidence predictions or intrinsically disordered. Plots are annotated to show the location of the intracellular loops (ICLs), extracellular loops (ECLs), and N- and C-termini for B2AR and canonical 14-3-3 binding residues.

Figure 4

14-3-3 protein inhibition increases cAMP levels after B2AR stimulation. A) HEK293 cells transfected with cAMP GloSensor and YFP-difopein (blue) or a YFP-R18 K-mutant negative control peptide (grey) show an increase in luminescence after treatment with 10 µM isoproterenol (Iso, dotted line; n=4, mean ± standard deviation). B) Concentration-response curve of GloSensor luminescence area under the curve (AUC) for the first 30 minutes after isoproterenol or media vehicle (Veh) treatment in HEK293 cells transfected with difopein or the control peptide. Values are shown as a percent of the response for cells expressing the control peptide treated with 10 µM iso (n=4, mean ± 95% confidence interval, values fit to a three-parameter non-linear regression, Extra sum-of-squares F-test: p<0.0001). C) HEK293 cells expressing difopein or the control peptide show an increase in GloSensor luminescence in response to treatment with 10 µM forskolin (Fsk, dotted line; n=4, mean ± standard deviation) D) Bar charts showing AUC for the first 30 minutes of treatment with 10 µM fsk in cells expressing difopein or the control peptide (n=4, mean ± 95% confidence interval, paired, two-tailed Student's t-test: p=0.0415).

Figure 5

14-3-3 proteins impair miniG protein recruitment to B2AR. A) Schematic demonstrating the NanoBit assay for miniGs recruitment to B2AR. Association of SmBit-miniGs with B2AR-LgBit increases NanoBit luminescence. B) Traces showing corrected NanoBit signal in HEK293 cells transfected with B2AR-LgBit, SmBit-miniGs, and either mCherry-difopein (blue) or the mCherry-tagged R18 Kmut control peptide before and for the first 30 minutes after stimulation with 10 µM isoproterenol (Iso; dotted line). Mean traces ± standard deviation of 4 independent experiments scaled to the peak of the control peptide condition. C) Concentration-response curve showing peak luminescence at increasing concentrations of isoproterenol (iso) or media vehicle (Veh) for cells expressing mCherry-difopein or the control peptide (mean ± 95% confidence interval, n=4).

Mean peak luminescence values were fit to a three-parameter non-linear regression (Extra sum-of-squares F-test comparing whether the two data sets are best fit by a single or by different curves: $p<0.0001$). D) Bar graph comparing baseline NanoBit luminescence values in cells expressing mCherry-difopein and the control peptide (mean ± 95% confidence interval, n=4, paired Student's t-test, p=0.0182).

Figure 6

Inhibiting 14-3-3 proteins promotes arrestin recruitment to B2AR. A) Recruitment of β-arrestin 2-SmBit to B2AR-LgBit after stimulation with an agonist results in an increase in NanoBit luminescence. B) NanoBit signal in HEK293 cells transfected with B2AR-LgBit, β-arrestin 2-SmBit, and either mCherry-difopein (blue) or an mCherry-R18 Kmut control peptide (grey). Luminescence rapidly increases following addition of 10 µM isoproterenol (dotted line) then declines. Mean traces ± standard deviation of 3 independent experiments scaled to the peak of the control peptide condition. C) Concentration-response curve of peak luminescence with increasing concentrations of isoproterenol or media vehicle (Veh) for cells expressing difopein or control peptide fit to a three-parameter non-linear regression (mean ± 95% confidence interval, n=3, Extra sum-of-squares F-test comparing whether the two data sets are best fit by a single or by different curves: $p<0.0001$). D) Bar chart showing baseline B2AR-arrestin NanoBit signal in cells transfected with difopein or control peptide (mean ± 95% confidence interval, n=3, paired, two-tailed Student's t-test: p=0.026).

Figure 7

14-3-3 proteins do not regulate B2AR-stimulated ERK phosphorylation. A) Western blot of phosphorylated ERK (pERK) and total ERK in FLAG-B2AR stably-expressing HEK293 cells transfected with either YFP-difopein or YFP-R18 K-mut control peptide stimulated with 10 µM

isoproterenol for 2-20 minutes or no treatment (NT). B) Quantification of the ratio between phosphorylated ERK and total ERK by treatment time, shown as a percent of the peak response for cells expressing the control peptide (n=4, mean ± standard deviation). C) Phosphorylated ERK to total ERK ratio after two minutes of treatment with isoproterenol (n=4, mean ± 95% confidence interval, paired, two-tailed t-test, p=0.608).

Figure 8

Proposed model of 14-3-3 regulation of B2AR function. 14-3-3 proteins bind to B2AR at the plasma membrane and impair interaction with effectors such as G proteins and arrestin, enforcing a sequestered reserve unavailable for immediate activation. Unbound B2AR is available to be activated and produce downstream signaling. Internalization following stimulation removes B2AR from the plasma membrane and reduces interaction with 14-3-3 proteins.
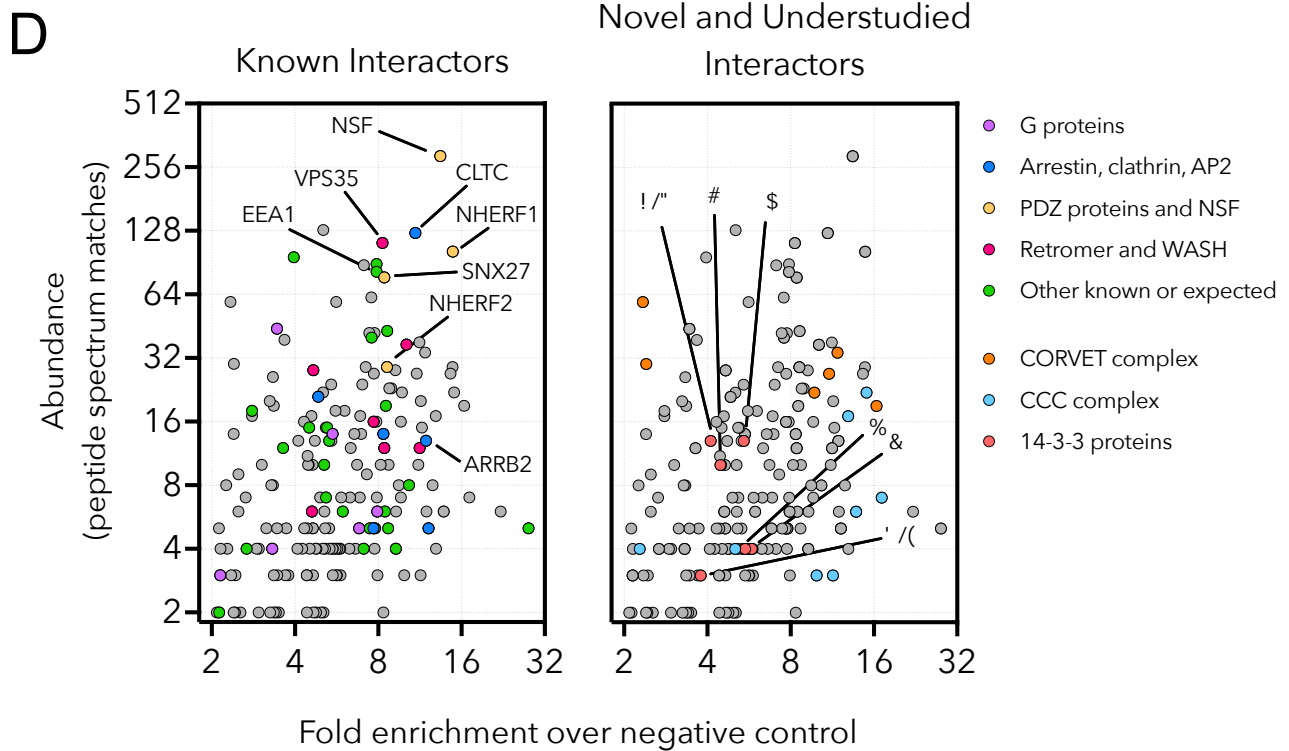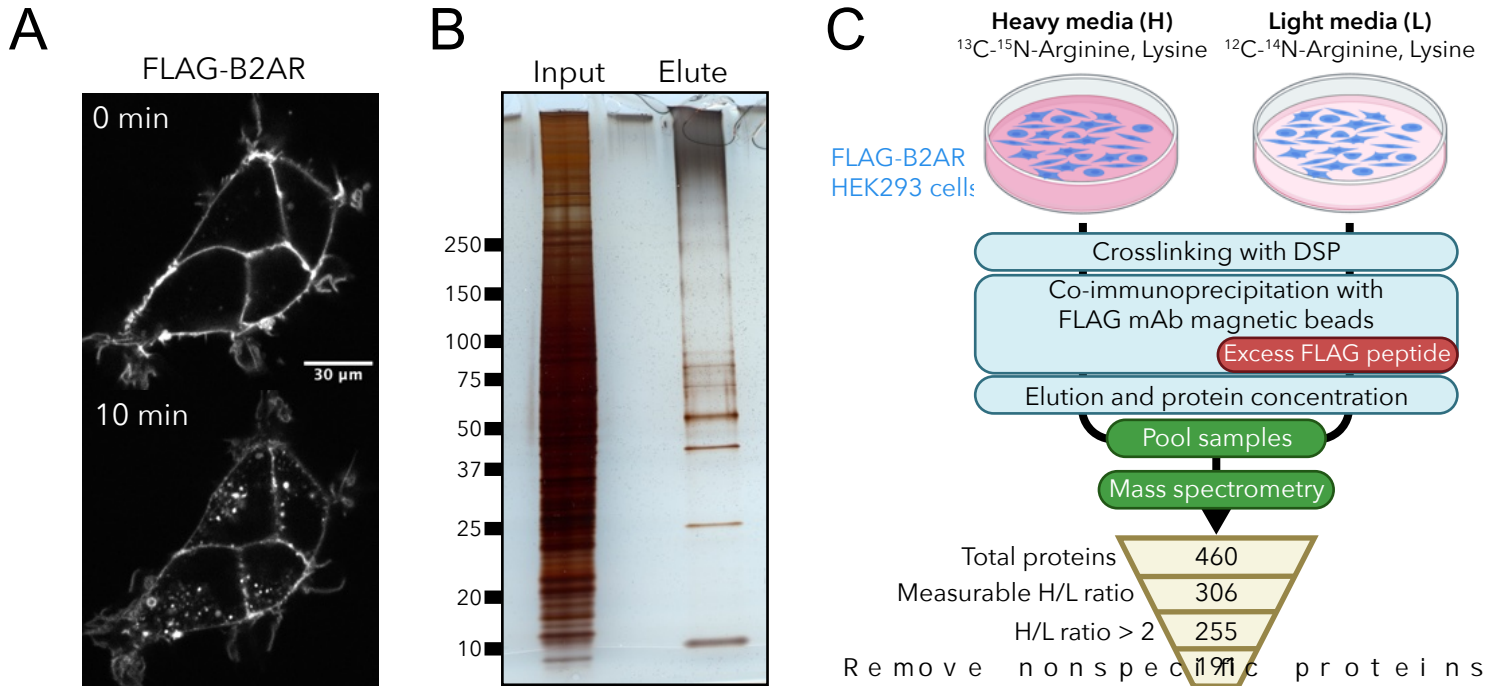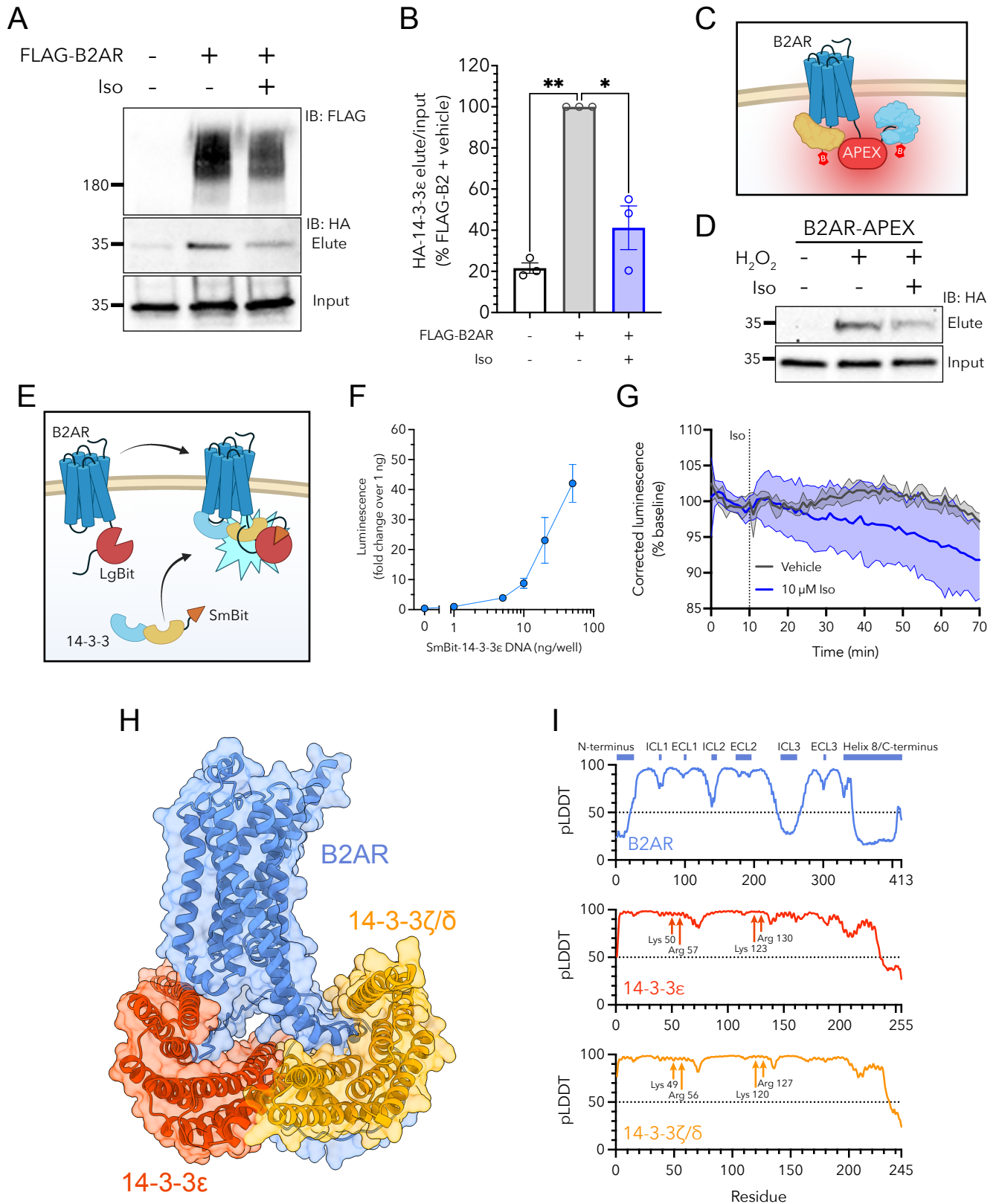
Figure 1

A

FLAG-B2AR

0 min

10 min

30 μm

B

Input   Elute

250
150
100
75
50
37
25
20
10

C

Heavy media (H)
^{13}C-^{15}N-Arginine, Lysine

Light media (L)
^{12}C-^{14}N-Arginine, Lysine

FLAG-B2AR HEK293 cells

Crosslinking with DSP

Co-immunoprecipitation with FLAG mAb magnetic beads

Excess FLAG peptide

Elution and protein concentration

Pool samples

Mass spectrometry

Total proteins	460
Measurable H/L ratio	306
H/L ratio > 2	255
Remove nonspecific proteins	191

D

Known Interactors

Abundance (peptide spectrum matches)

512
256 — NSF
128 — VPS35, CLTC
EEA1 — NHERF1
64 — SNX27
32 — NHERF2
16
8 — ARRB2
4
2

Novel and Understudied Interactors

! /"   # $
% &
' /(

- ● G proteins
- ● Arrestin, clathrin, AP2
- ● PDZ proteins and NSF
- ● Retromer and WASH
- ● Other known or expected
- ● CORVET complex
- ● CCC complex
- ● 14-3-3 proteins

Fold enrichment over negative control

2   4   8   16   32

Figure 2

Figure 3

Figure 4

Figure 5

Figure 6

A

B

C

Figure 7

Figure 8